Sensors & Actuators: A. Physical 405 (2026) 117797

Contents lists available at ScienceDirect

Sensors and Actuators: A. Physical

journal homepage: www.journals.elsevier.com/sensors-and-actuators-a-physical

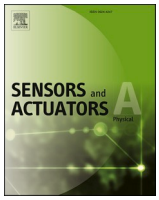

Terahertz multiband metamaterial biosensor for ultrasensitive detection of PC-12 adrenal gland carcinoma cells through microenvironmental analysis

Musa N. Hamza [a,*], Mohammad Alibakhshikenari [b,c,**], Bal Virdee [d], Sunil Lavadiya [e], Iftikhar ud Din [f,g], Bruno Sanches [g], Slawomir Koziel [h,i], Syeda Iffat Naqvi [j], Ali Farmani [k], Abinash Panda [l], Hassan Zakeri [m], Nisar Ahmad Abbasi [n]

[a] Department of Physics, College of Science, University of Raparin, Sulaymaniyah 46012, Iraq
[b] Lero, the Research Ireland Centre for Software, College of Science and Engineering, School of Computer Science, University of Galway, Galway H91 TK33, Ireland
[c] Department of Electrical and Electronics Engineering, Dogus University, Umraniye, Istanbul 34775, Türkiye
[d] Center for Communications Technology, London Metropolitan University, London N7 8DB, UK
[e] Department of Information and Communication Technology, Marwadi University, Rajkot, Gujarat 360003, India
[f] Telecommunication Engineering Department, University of Engineering and Technology, Mardan 23200, Pakistan
[g] Department of Electronic Systems Engineering, Escola Politécnica da Universidade de São Paulo, São Paulo, Brazil
[h] Engineering Optimization & Modeling Center, Reykjavik University, Reykjavik 102, Iceland
[i] Faculty of Electronics, Telecommunications and Informatics, Gdansk University of Technology, Gdansk 80-233, Poland
[j] Department of Telecommunication Engineering, University of Engineering & Technology, Taxila, Pakistan
[k] Department of electronics engineering, Lorestan university, Iran
[l] Department of Electronics and Communication Engineering, CMR Institute of Technology, Bengaluru 560037, India
[m] Department of Electrical Engineering, Amirkabir University of Technology, Tehran 15875-4413, Iran
[n] Department of Electrical Engineering, School of Systems Engineering, Bahrain Polytechnic, Isa Town, Bahrain

ARTICLE INFO

Keywords:
Biosensor
Metamaterial
Terahertz
Cancer detection
Early-stage diagnosis
Microenvironmental analysis

ABSTRACT

Adrenal gland cancer, particularly adrenocortical carcinoma (ACC), is an aggressive malignancy arising from the adrenal cortex's secretory cells. ACC is often diagnosed at advanced, metastatic stages, necessitating surgical resection. However, its high recurrence rate and late-stage detection frequently require systemic therapies, which are generally ineffective, leading to poor survival outcomes. Early detection is, therefore, crucial for improving treatment efficacy. Identifying PC-12 adrenal gland carcinoma cells is essential for understanding neuroendocrine tumor progression and developing effective therapeutic strategies. This study presents a novel metamaterial (MTM)-based biosensor for detecting PC-12 carcinoma cells with exceptional sensitivity. The sensor features three resonators fabricated on 0.2-μm-thick aluminum (Al) layers embedded within a 10-μm-thick polyethylene terephthalate (PET) substrate. The sensor is highly compact with an overall dimension of just 150 × 150 μm², making it well-suited for integration into portable diagnostic systems. Operating in the terahertz frequency range (0.5 THz to 5.0 THz), the device achieves remarkable performance, with an absorption rate exceeding 99% across eight operating bands and surpassing 99.9% in two bands. Additionally, it boasts high quality factor (approaching 30) and an exceptional sensitivity of nearly 4000,000 THz/RIU. The sensor's outstanding performance is attributed to meticulous geometric tuning and architectural optimization, significantly enhancing its sensitivity for cancer detection. Numerical validation was conducted using full-wave electromagnetic simulations, including electric and magnetic field distribution analysis, surface current mapping, and scattering parameter evaluation. Comparative assessments against state-of-the-art biosensors demonstrated the proposed sensor's superiority in key performance metrics such as quality factor, figure of merit (FOM), and absorption efficiency. The sensor's efficacy in detecting PC-12 adrenal carcinoma cells was verified by integrating it into a

* Corresponding author.
** Corresponding author at: Lero, the Research Ireland Centre for Software, College of Science and Engineering, School of Computer Science, University of Galway, Galway H91 TK33, Ireland.
E-mail addresses: musa.nuraden@uor.edu.krd (M.N. Hamza), mohammad.alibakhshikenari@universityofgalway.ie (M. Alibakhshikenari), b.virdee@londonmet.ac.uk (B. Virdee), sunil.lavadiya@marwadieducation.edu.in (S. Lavadiya), Iftikhar.Ud.Din@uqtr.ca (I. Din), bruno.csanches@usp.br (B. Sanches), koziel@ru.is (S. Koziel), iffat.naqvi@uettaxila.edu.pk (S.I. Naqvi), farmani.a@lu.ac.ir (A. Farmani), abinash.p@cmrit.ac.in (A. Panda), h.zakeri@aut.ac.ir (H. Zakeri), nisar.abbasi@polytechnic.bh (N.A. Abbasi).

https://doi.org/10.1016/j.sna.2026.117797
Received 10 June 2025; Received in revised form 11 March 2026; Accepted 30 March 2026
Available online 31 March 2026

Microwave Imaging (MWI) system. The device successfully distinguished between healthy and cancerous cells by capturing distinct electromagnetic signatures through electric (E) and magnetic (H) field variations. These results underscore the sensor's potential as a highly sensitive, non-invasive diagnostic tool for early-stage detection of adrenal gland cancer and other malignancies.

1. Introduction

The adrenal gland consists of two main regions: the cortex, which secretes steroid hormones, and the medulla, which produces catecholamines. Hormones derived from the adrenal gland play a crucial role in regulating essential physiological functions such as stress response, blood pressure, and metabolism. Various tumors, both benign and malignant, can develop in the adrenal glands. Among them, adrenocortical carcinoma (ACC), a highly aggressive cancer originating from the secretory cells of the adrenal cortex, has an incidence rate of 0.5–2 cases per million. Similarly, pheochromocytomas (PCCs), which arise from the chromaffin cells of the adrenal medulla, occur at a rate of 0.8 cases per million annually [1,2]. ACC is commonly diagnosed at advanced and metastatic stages. Although surgical resection is the preferred treatment, the high recurrence rate and late-stage detection often necessitate systemic therapies, which remain largely ineffective, resulting in a survival rate of less than 44% [3].

In recent years, progress in adrenal cancer research has been facilitated by the development of improved in vitro and computational models, enabling more accurate representation of tumor heterogeneity and disease progression. However, despite advances in molecular biology and oncology, early-stage diagnosis of adrenal malignancies remains a major clinical challenge. PCCs, while predominantly benign, are strongly influenced by genetic background and molecular classification, with malignancy occurring in approximately 10% of cases. If left untreated, excessive catecholamine secretion can lead to severe cardiovascular complications [4]. Metastasis occurs in fewer than 15% of cases, while recurrence rates following surgical resection range from 6% to 16%, depending on tumor size and genetic factors [5,6]. Importantly, all PCCs are considered potentially metastatic, as no definitive biomarkers reliably predict malignant transformation [7].

Early detection of adrenal gland cancer is therefore critical for improving patient outcomes and reducing healthcare burdens. Current diagnostic approaches rely on a combination of imaging techniques—such as computed tomography (CT), magnetic resonance imaging (MRI), positron emission tomography (PET-CT), and ultrasound—alongside biochemical testing, histopathology, and genetic or molecular analyses [8–15]. Despite their clinical utility, these methods suffer from significant limitations. Imaging modalities often struggle to distinguish benign from malignant lesions and may yield false positives or negatives, particularly for small tumors [16,17]. CT and PET scans involve ionizing radiation or radioactive tracers, while MRI and PET remain costly and inaccessible in many healthcare settings. Biochemical testing is similarly confounded by physiological stress, hypertension, and other neuroendocrine disorders, often necessitating repeated or confirmatory tests that delay diagnosis [18,19]. Genetic testing, while promising, is expensive and lacks universal predictive power, as not all adrenal cancers exhibit identifiable pathogenic mutations [20,21]. These challenges highlight the urgent need for alternative diagnostic strategies that are rapid, non-invasive, sensitive, and widely accessible.

The detection and analysis of PC-12 adrenal gland carcinoma cells are particularly important for understanding neuroendocrine tumor behavior and therapeutic response [22]. Conventional techniques such as immunocytochemistry, flow cytometry, and fluorescence-based assays provide valuable molecular insights but are limited in their ability to capture dynamic cellular behavior and real-time microenvironmental interactions [23–25]. To address these limitations, Dynamic Microenvironment Profiling (DMP) has emerged as a promising diagnostic paradigm, enabling real-time monitoring of cellular responses, biochemical signaling, and biomechanical properties associated with malignant transformation [26,27]. DMP focuses on how tumor cells interact with their surrounding microenvironment, allowing differentiation between benign and malignant phenotypes based on dynamic behavior rather than static biomarkers alone.

Effective implementation of DMP requires highly sensitive sensing platforms capable of detecting minute changes in cellular dielectric properties. In this context, terahertz (THz) sensing technologies have gained increasing attention due to their strong sensitivity to water content, biomolecular composition, and cellular structure, while remaining non-ionizing and label-free. Recent studies have demonstrated the effectiveness of THz photonic crystal fiber (PCF) and refractive-index-based sensors for detecting a wide range of cancer cells, including breast, cervical, brain, blood, and adrenal gland cancers, with exceptionally high sensitivity and low loss characteristics. These works highlight the ability of THz-based photonic structures to distinguish healthy and malignant cells through subtle refractive index variations, reinforcing their potential for early cancer diagnostics.

Metamaterials—artificially engineered structures exhibiting electromagnetic properties not found in nature—offer additional advantages for biosensing applications, including extreme field confinement, tunable resonances, and miniaturization [28,29]. When functionalized for biological detection, metamaterial-based sensors amplify local refractive index changes induced by biomolecular interactions, resulting in highly sensitive resonance shifts. Operating in the terahertz regime, such sensors enable non-destructive, label-free analysis and are well suited for integration with DMP frameworks. Recent advances have demonstrated successful application of THz and GHz metamaterial and photonic sensors for detecting multiple cancer types and disease conditions, underscoring their versatility and diagnostic potential [30–69].

Recent advances in terahertz and photonic crystal fiber–based biosensing have demonstrated high sensitivity for detecting various cancer cells through refractive-index contrast, including adrenal gland carcinoma, brain tumors, leukemia, and other malignancies. For example, THz photonic crystal fiber sensors have been reported for adrenal and breast cancer detection [70], early-stage brain tumor identification [71], Jurkat (leukemia) cell discrimination [72], and brain lesion diagnosis using THz refractive-index sensing [73]. These studies validate the feasibility of THz-based dielectric sensing for cancer diagnostics and motivate the development of metamaterial-based alternatives with enhanced absorption and multiband response [74–78].

In this study, we present a terahertz metamaterial-based biosensor for ultrasensitive detection of PC-12 adrenal gland carcinoma cells. The proposed sensor incorporates three resonators embedded in a 10-μm-thick polyethylene terephthalate (PET) substrate with 0.2-μm-thick aluminum layers, achieving absorption exceeding 99% across multiple frequency bands. The design exhibits a high-quality factor (~30), exceptional sensitivity (~4000,000 THz/RIU), and superior figure of merit (FOM), as validated through full-wave electromagnetic simulations. Furthermore, integration with a microwave imaging (MWI) framework demonstrates the sensor's ability to distinguish healthy and cancerous cells, highlighting its potential as a non-invasive, high-performance diagnostic platform for early-stage adrenal gland cancer detection.

2. Design and electromagnetic configuration of metamaterials

This section explores the structural and electromagnetic properties of the proposed metamaterial system, emphasizing its design evolution and

functional characteristics. Metamaterials are artificially engineered structures designed to exhibit electromagnetic properties not typically found in natural materials. Their unique behavior arises from the periodic arrangement of subwavelength resonators, such as split-ring resonators, which enable precise manipulation of electromagnetic waves.

The design process involves selecting an appropriate unit cell structure and material composition to achieve the desired electromagnetic response at specific frequencies. The effective permittivity and permeability of the metamaterial can be tailored to produce phenomena such as negative refractive indices, cloaking effects, or super-lensing. Computational techniques, including finite element analysis (FEA) and finite-difference time-domain (FDTD) simulations, are employed to optimize the metamaterial's performance across different wavelength regimes, from microwave to optical frequencies.

Furthermore, the electromagnetic configuration is analyzed to understand how the designed structure interacts with incident electromagnetic waves. The absorption mechanism is examined in detail, focusing on the spatial arrangement and geometry of the resonators, which play a crucial role in tuning the metamaterial's response. Through careful engineering, the proposed metamaterial is optimized for high-efficiency wave absorption, making it suitable for applications such as perfect absorbers.

2.1. Structural Framework of Metamaterials (MTMs)

The proposed Terahertz Multiband Metamaterial Biosensor is designed as a multilayered structure incorporating metamaterials (MTMs) and various surface materials, including aluminum (Al), polyethylene terephthalate (PET), a PC-12 coverslip, and adrenal gland cells. The configuration is schematically represented in Fig. 1, where structural parameters H, I, J, and K (Table 1) define the external and internal geometric features of the substrate. The aluminum layer, with a thickness of 0.2 μm, serves as a conductive surface, while the PET dielectric layer (T1) is 10 μm thick, ensuring stable wave propagation. The PC-12 coverslip (T2) measures 2 μm, and the layer containing PC-12 adrenal gland cells (T3) is 8 μm, all contributing to the structural integrity of the MTM waveguide.

The sensor is designed to operate within the terahertz frequency range of 0.5–5 THz, where incident waves interact with the metamaterial surface to achieve near-perfect absorption. The amplitude of the incident THz wave is coupled to the structured surface, facilitating an optimal absorption mechanism that minimizes reflections and enhances sensing capabilities. Within this configuration, PET functions as the waveguide medium, characterized by a refractive index n_{PET}, while the aluminum components provide high conductivity and minimal electromagnetic losses, with a refractive index n_{Al}. Figs. 1(a) and 1(b) present the initial design and its proposed modifications, while Figs. 2(a) and 2(b) illustrate the integration of secondary and tertiary resonators,

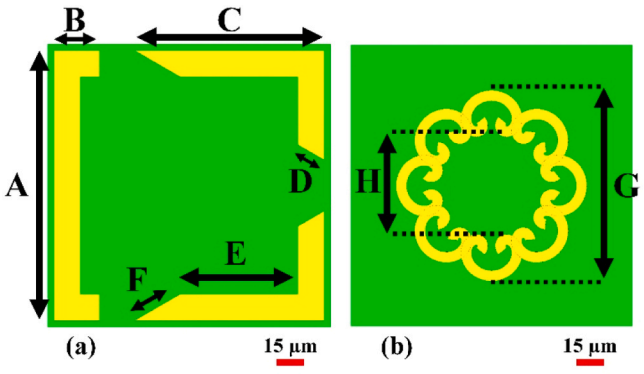

Fig. 1. Schematic representation of the proposed metamaterial-based absorber: (a) Initial resonator structures; (b) Secondary resonator configurations.

Table 1
Summary of Optimized Parameters for the Proposed Biosensor Configuration.

Parameter	Value (μm)	Parameter	Value (μm)
A	142.84	H	56
B	23.92	I	33
C	100.12	J	49
D	15.92	K	150
E	62.45	Aluminum (Al) thick	0.2
F	27.58	PET thick (T1)	10
G	101	Coverslip thick (T2)	2
		PC-12 Adrenal Gland Cells thick (T3)	8

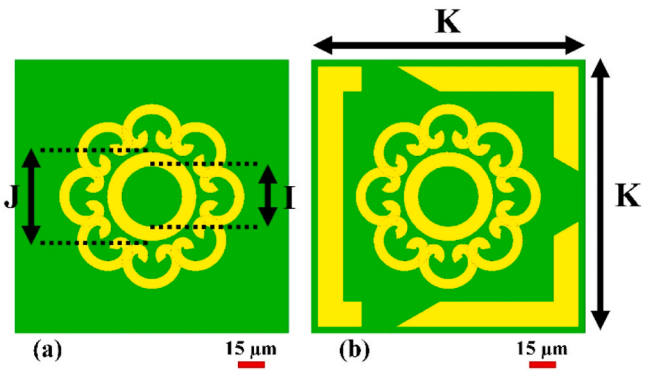

Fig. 2. Complete metamaterial architecture: (a) Integration of secondary and tertiary resonators; (b) Finalized structural model.

culminating in the finalized structural model.

The metamaterial architecture consists of a tri-layered system where two thin aluminum layers encapsulate a PET dielectric spacer. The aluminum layers, each with a thickness of 0.2 μm and a conductivity of 3.56×10^7 S.m^{-1}, function as an impedance-matched surface to facilitate wave penetration while simultaneously acting as a reflective barrier to prevent transmission losses. The absorption process is governed by both electrical and magnetic loss mechanisms, optimizing energy confinement and enhancing biosensing sensitivity.

To evaluate the electromagnetic performance of this metamaterial, numerical simulations were performed using CST Studio Suite with the frequency-domain finite element solver, ensuring precise characterization of resonance behavior across different structural configurations. Periodic (unit cell) boundary conditions were applied along the *x*- and *y*-directions to emulate an infinite array, while open (add space) boundaries with perfectly matched layers (PMLs) were implemented along the *z*-direction to suppress artificial reflections. A normally incident plane wave excitation was used. Local mesh refinement was applied around sharp metallic edges and thin dielectric layers to accurately resolve electromagnetic field distributions.

To exclude numerical artifacts, extensive convergence testing was performed. Mesh refinement was continued until resonance frequencies and linewidths varied by less than 1% between successive refinement steps. High-resolution frequency sampling was used near resonance peaks to ensure accurate FWHM extraction. Boundary conditions and PML thickness were varied to confirm resonance stability without significant frequency drift. Energy conservation was verified using $A = 1 - |S_{11}|^2 - |S_{21}|^2$, ensuring physically consistent absorption values across the full spectrum.

Additional numerical verification was performed using CST's adaptive mesh refinement. Multiple refinement passes were executed until convergence was achieved, defined by resonance frequency variation below 1% and negligible change in S-parameters between successive iterations. These criteria ensured numerical stability and reproducibility of the reported resonance characteristics, independent of mesh density.

Accurate THz illumination requires precise alignment of wave

excitation sources, whether plane waves or port-based inputs, with the designated polarization state. Optimization strategies such as leveraging symmetry planes and defining material properties with high accuracy further enhance the simulation's efficiency. Post-processing techniques enable comprehensive analysis of absorption spectra and electric field distributions, providing insights into the metamaterial absorber's operational effectiveness.

By tuning key structural parameters—including geometric dimensions and material properties—metamaterial absorbers can be engineered for application-specific resonance characteristics. Functionalizing the sensor surface with biomolecular receptors enhances selectivity, enabling the detection of molecular spectral signatures through biomolecular interactions. The integration of high-absorption metamaterials at precise THz frequencies offers a label-free, real-time sensing platform. These advancements in metamaterial-based biosensing have significant potential for biomedical diagnostics, providing a powerful tool for detecting molecular vibrational signatures with exceptional sensitivity and specificity.

2.2. Electromagnetic configuration and absorption mechanism

The proposed terahertz (THz) multiband metamaterial biosensor is designed for the detection of PC-12 adrenal gland cancer cells through the interaction of incident electromagnetic waves with a precisely engineered metamaterial structure. The sensor consists of an array of metamaterial perfect absorbers (MTM-PAs) fabricated from aluminum (Al) patterns deposited onto a polyethylene terephthalate (PET) substrate, as illustrated in Fig. 3. The periodic arrangement of these structures ensures efficient resonance coupling, with the incident wave characterized by its electric field, magnetic field, and wave vector. Key parameters affecting the resonant absorption include the angle of incidence and polarization, which enable precise tuning of the sensor's response. The resulting multiple resonance frequencies correspond to distinct absorption peaks within the THz spectrum, ensuring high sensitivity to dielectric variations induced by biological analytes.

The absorption mechanism within the biosensor is primarily governed by the excitation of localized surface plasmon resonances (LSPRs) and Fabry-Pérot cavity modes. The structured aluminum resonators function as frequency-selective elements, confining electromagnetic energy to specific THz frequencies. This interaction generates strong electric field localization, enhancing absorption efficiency. The PET substrate, serving as a low-loss dielectric medium, contributes to resonance stability and minimizes unwanted energy dissipation. As a result, the metamaterial system achieves near-unity absorption at designated frequencies, a critical feature for biosensing applications where even minor dielectric perturbations lead to measurable shifts in resonance characteristics.

Dynamic resonance frequency analysis enables precise detection of PC-12 adrenal gland cancer cells by monitoring shifts in the effective refractive index upon cell attachment to the metamaterial surface. Changes in the local dielectric environment induce detectable frequency shifts, providing a quantitative measure of cellular presence and concentration. The controlled orientation of the incident electromagnetic wave enhances sensitivity by optimizing coupling conditions and facilitating interaction with target analytes. Additionally, the biosensor's multiband resonance properties allow simultaneous detection of multiple biomolecular variations, further improving selectivity. This advanced metamaterial design thus establishes an efficient platform for label-free, ultrasensitive cancer cell detection, with significant potential for real-time biomedical diagnostics.

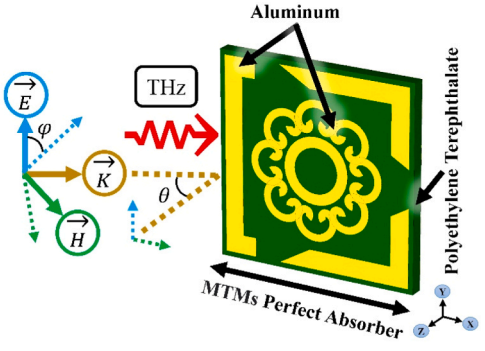

Fig. 3. Illustration of the structural setup along with the orientation of the incident electromagnetic field.

To evaluate fabrication robustness, key geometric parameters of the resonators were varied within realistic lithographic tolerances (±1–5 μm). The resonance peaks remained clearly observable, exhibiting primarily predictable frequency shifts and minor variations in absorption amplitude rather than disappearance or distortion. This behavior confirms that the resonances are intrinsic to the metamaterial design and that the sensing mechanism based on dielectric loading–induced resonance shifts remain stable under practical dimensional deviations.

3. Optimization and performance assessment of absorptive properties

The absorptive properties of metamaterial-based structures play a crucial role in determining their efficiency for various applications, particularly in biosensing and electromagnetic wave manipulation. To achieve optimal absorption characteristics, a comprehensive evaluation of different design configurations, material compositions, and geometric parameters is essential. This section presents a systematic approach to optimizing the absorptive performance of the proposed metamaterial structure through comparative analysis, material selection, and structural refinement.

Initially, a comparative study of different structural configurations is conducted to assess their influence on absorptive behavior. The impact of design variations on absorption efficiency is analyzed, providing insight into the key geometrical parameters that enhance performance. Subsequently, the effect of substrate and resonator materials is examined, where various dielectric substrates and metallic resonators are evaluated to determine their contributions to absorption enhancement. Finally, the influence of substrate thickness is investigated to identify the optimal configuration for achieving maximum absorption across the desired frequency spectrum.

The following subsections detail the optimization strategies and performance assessment methodologies, supported by graphical representations of absorption spectra and comparative analyses of different configurations.

3.1. Comparative analysis of different structural configurations

Fig. 4 presents the relative absorptive response of two distinct metamaterial designs intended for THz multiband biosensing applications. Within the 0.5–5.0 THz range, the absorption spectra illustrate how structural modifications influence resonance properties. Fig. 4(a) corresponds to Design Variation 1, where the resonator shape exhibits multiple high-frequency oscillations, leading to a distributed arrangement of absorption peaks. The structural architecture of Fig. 4(a), highlighted in the inset, features a simplified rectangular framework. The variation in absorption strengths across the frequency spectrum suggests highly unstable resonance behavior in this design. The absence of well-defined absorption peaks indicates less effective energy coupling and weaker field confinement, which may limit the sensor's sensitivity to biological variations.

Conversely, Fig. 4(b) corresponds to Design Variation 2, which exhibits significantly improved absorption efficiency due to a more complex and symmetric resonator structure. The presence of well-defined,

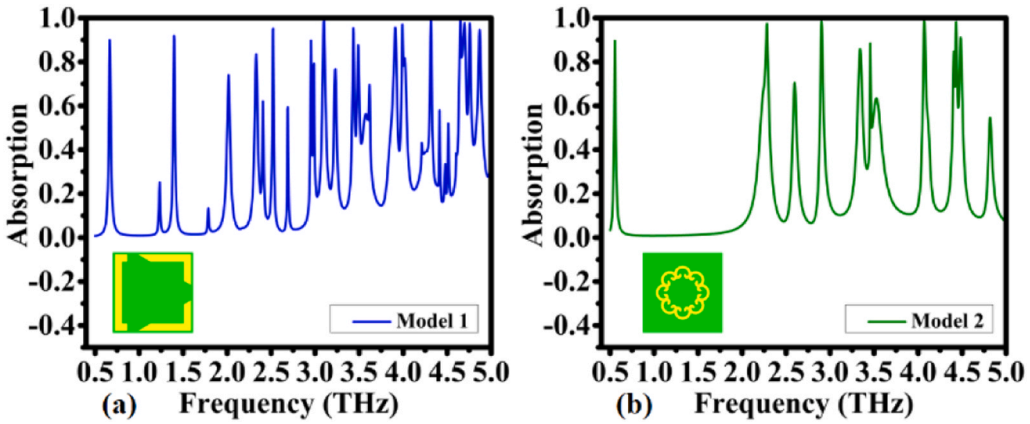

Fig. 4. Absorptive response comparison between two configurations: (a) Design Variation 1; (b) Design Variation 2.

distinct peaks in the absorption spectra at multiple THz frequencies indicates superior resonance stability. The enhanced structural arrangement shown in the inset of Fig. 4(b) consists of a circular resonator with embedded patterns, facilitating localized surface plasmon resonance (LSPR). This architecture ensures stronger interactions with incident THz waves by enhancing electromagnetic field confinement. The reduced spectral noise and more pronounced absorption peaks of this model indicate increased sensitivity, making it more suitable for precise biosensing applications.

A comparative analysis of these two structural configurations reveals that design complexity directly influences absorptive response. Design Variation 2 exhibits well-defined, high-Q factor resonances that enhance detection capabilities, whereas Design Variation 1 presents broader resonance distributions with fluctuating intensities. The improved absorption characteristics of the second design are particularly critical for biosensing applications, as they enable more precise detection of dielectric fluctuations associated with PC-12 adrenal gland carcinoma cells. These findings highlight the importance of structural optimization in metamaterial-based biosensors to achieve superior performance in biomedical diagnostics.

Fig. 5 evaluates the absorptive performance of two additional metamaterial structures, further demonstrating how structural variations affect resonance behavior in the THz spectrum. These models are assessed for their ability to optimize absorption properties, thereby enhancing biosensing capability. Fig. 5(a) corresponds to Design Variation 3, where the absorption spectra exhibit multiple resonant peaks distributed across the 0.5–5.0 THz frequency range. The inset of Fig. 5 (a) depicts a distinctive geometric pattern designed to enhance localized surface plasmon resonance (LSPR) effects. Although this arrangement supports multiple resonances, the measured absorption profile indicates that certain peaks exhibit reduced absorption efficiency, which may limit its sensitivity in detecting small dielectric variations induced by biological analytes.

Employing a more refined resonator configuration, Fig. 5(b) illustrates the absorptive response of Design Variation 4, demonstrating a significantly enhanced absorption profile. Strong electromagnetic field confinement, as indicated by well-defined and sharp resonance peaks, improves interactions with incident THz waves. The more complex resonator design in Fig. 5(b) supports enhanced resonance stability and absorptive strength across multiple THz frequencies. Compared to Design Variation 3, this model exhibits superior absorption efficiency, fewer variations, and a more consistent spectral response, making it a more attractive choice for high precision biosensing applications.

A comparative analysis of these additional models underscores the critical role of resonator geometry in determining the absorption properties of metamaterial-based biosensors. While Design Variation 3 provides broad spectral coverage with multiple peaks, its absorption strength remains inconsistent, potentially affecting sensing reliability. In contrast, Design Variation 4 demonstrates a more stable and efficient absorption profile, which is essential for detecting variations in the biological microenvironment. These results further validate the necessity of structural optimization in metamaterial absorbers to ensure maximal sensitivity in detecting PC-12 adrenal gland cancer cells.

3.2. Influence of substrate and resonator materials on absorption efficiency

The absorption properties of metamaterials (MTMs) are greatly influenced by the materials used in their composition. To determine the appropriate material selection, the impact of both substrate and

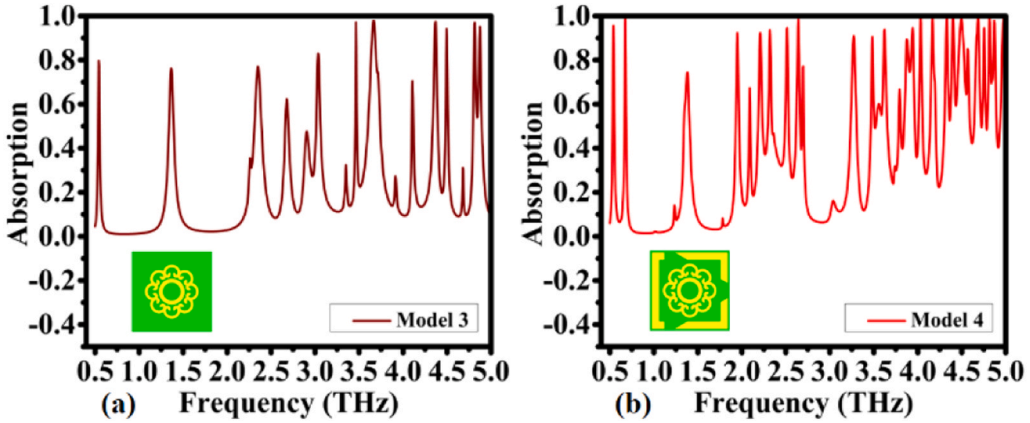

Fig. 5. Absorptive performance assessment of additional models: (a) Design Variation 3; (b) Design Variation 4.

resonator materials was analyzed, aiming to achieve a balance between practicality, usability, and performance attributes.

The 0.5–5.0 THz range was selected as it offers an effective trade-off between penetration depth and sensitivity to dielectric variations in biological samples. While lower frequencies provide deeper penetration with reduced sensitivity and higher frequencies may enhance molecular specificity at the expense of higher attenuation, the chosen band represents a practical compromise; nevertheless, resonator retuning could enable optimization for specific biomarkers in future work.

The absorption characteristics of the proposed metamaterial design, utilizing various substrates such as Polyimide, Arlon AD 430, Rogers RT5870, and PET within the terahertz frequency range of 0–5 THz, are crucial in determining the material's performance, particularly in terms of absorptivity. The choice of substrate significantly influences the electromagnetic response, playing a key role in optimizing the design's effectiveness for high-frequency applications.

Polyimide, known for its high dielectric constant and low loss tangent, is commonly used in flexible electronics. Its absorption behavior varies across the terahertz spectrum, exhibiting three absorptivity peaks above 80% between 0.5 and 2 THz, four peaks above 80% from 2 to 3.5 THz, and a sharp increase in absorptivity peaks at higher frequencies from 3.5 to 5 THz. However, its high dielectric constant may slightly affect the coupling between electromagnetic waves and the substrate material, as illustrated in Fig. 6(a).

Arlon AD 430, a thermosetting laminate, is valued for its low dielectric constant and low loss tangent, making it a suitable choice for high-frequency applications. Its low loss tangent ensures minimal signal energy dissipation, thereby enhancing absorptivity, as depicted in Fig. 6 (b). The absorption characteristics of Arlon AD 430 are comparable to those of Polyimide within the same terahertz frequency range, with slight variations. However, it maintains a more stable absorption response as the frequency increases from 0 to 5 THz.

In Fig. 7(a), Rogers RT5870, known for its low dielectric loss and high glass transition temperature, is commonly used in microwave and millimeter-wave applications. Its low dielectric loss ensures efficient energy absorption within the proposed design, contributing to overall performance. The absorption spectra exhibit a low response with two peaks above 80% at lower frequencies from 0.5 to 2 THz, a moderate response with four peaks at middle frequencies from 2 to 3.5 THz, and sharp, well-defined absorption peaks at high frequencies from 3.5 to 5 THz due to its superior material properties.

On the other hand, Polyethylene Terephthalate (PET), a widely used polymer, has a low dielectric constant and low loss tangent, resulting in moderate energy dissipation. While PET's performance is like that of Rogers RT5870, it is more prominent at middle and high frequencies compared to Rogers RT5870. Its low loss tangent and dielectric constant still contribute to a decent level of absorption. The absorption spectra for PET exhibit a smoother and more gradual increase in absorptivity across the 0–5 THz range.

All four resonator metals such as Silver, Gold, Copper and Aluminum show absorption peaks above 80% across the terahertz range, indicating their effectiveness as resonator materials. However, the impact of the metal on overall design performance was found to be less significant compared to the variations resulting from different substrate materials. Figs. 8(a) and 8(b) illustrate the absorption characteristics of Silver and Gold. Due to their high conductivity, Silver and Gold demonstrate sharp surface plasmon resonances, leading to prominent absorption peaks within the THz frequency range of 0–5 THz, making them highly effective for determining slight variation in biological tissues for biosensing applications.

Additionally, the absorption properties of Copper and Aluminum as resonating materials contribute to enhancing the multiband capabilities of metamaterial biosensors. Copper, due to its high conductivity, and Aluminum, recognized for its lightweight nature and cost efficiency, both demonstrate notable absorption behavior within the terahertz frequency range of 0–5 THz, as shown in Figs. 9(a) and 9(b), respectively. These resonator materials facilitate a wide range of absorption frequencies, which is crucial for developing highly sensitive and selective multiband biosensors designed to detect tumors within the microenvironment.

The analysis presented in Figs. 10–11 examines the effect of substrate thickness on absorption efficiency within the 0.5–5 THz frequency range. Each figure illustrates varying substrate thicknesses and their corresponding responses, providing a comprehensive understanding of how different thickness levels influence the ability to absorb electromagnetic waves. A preliminary analysis of Fig. 10(a) and (b), which depict substrate thicknesses of 10 and 20 μm, reveals promising absorption performance across the entire frequency spectrum. This indicates that relatively thinner substrates exhibit enhanced absorption characteristics within the specified frequency range. A strong response suggests an efficient interaction between electromagnetic waves and the substrate, leading to effective absorption. For the proposed metamaterial biosensor, a thickness of 10 μm achieved an absorption efficiency exceeding 85% at the initial 0.5 THz, maintained a stable response in the mid-frequency range from 1.5 to 2.5 THz, and demonstrated sharp and consistent absorption at higher frequencies between 3 and 5 THz. In contrast, the 20 μm thickness presented a more stable response in the mid-frequency range from 1.5 to 4 THz but exhibited lower absorption at higher frequencies compared to the 10 μm substrate thickness.

Fig. 11 illustrates the impact of varying substrate thicknesses on absorption efficiency within the 0.5–5 THz frequency range. In Fig. 11 (a), a substrate thickness of 40 μm achieves absorption rates exceeding 80% at specific frequencies: 1.5, 2.5, and 4 THz, as well as within the

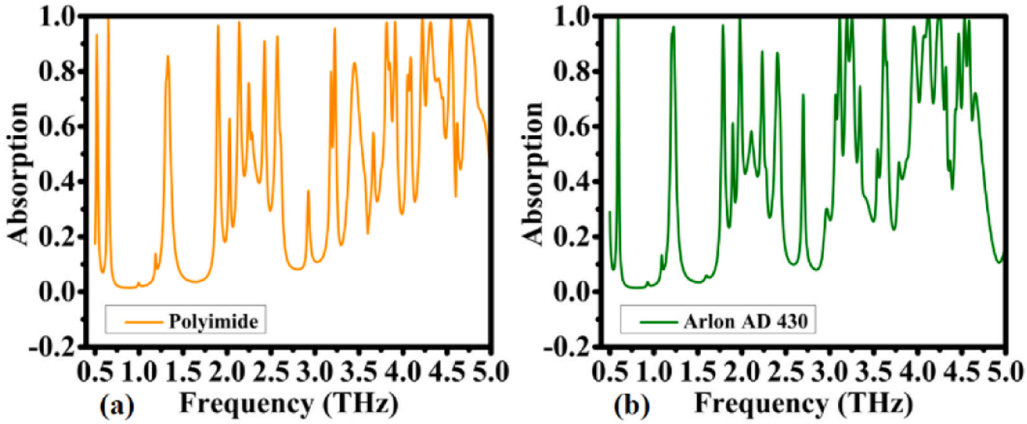

Fig. 6. Comparative absorption spectra for varying substrate materials: (a) Polyimide; (b) Arlon AD 430.

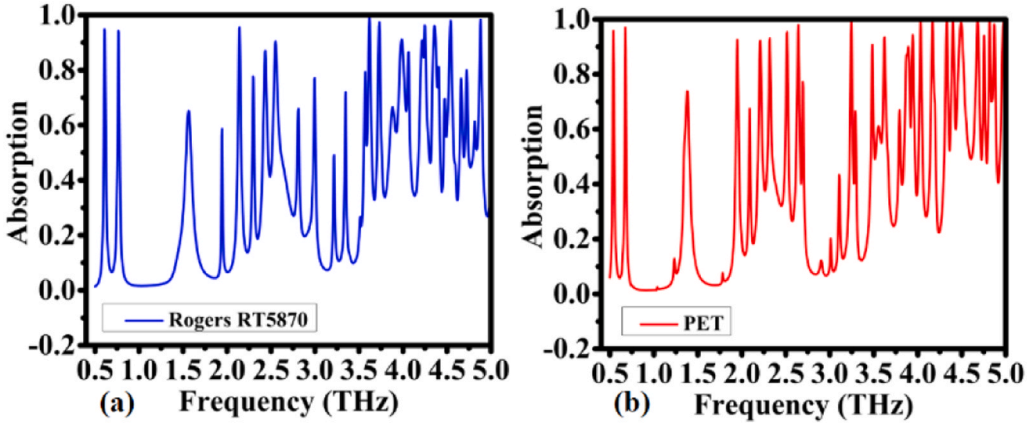

Fig. 7. Absorption performance with different substrates: (a) Rogers RT 5870; (b) PET.

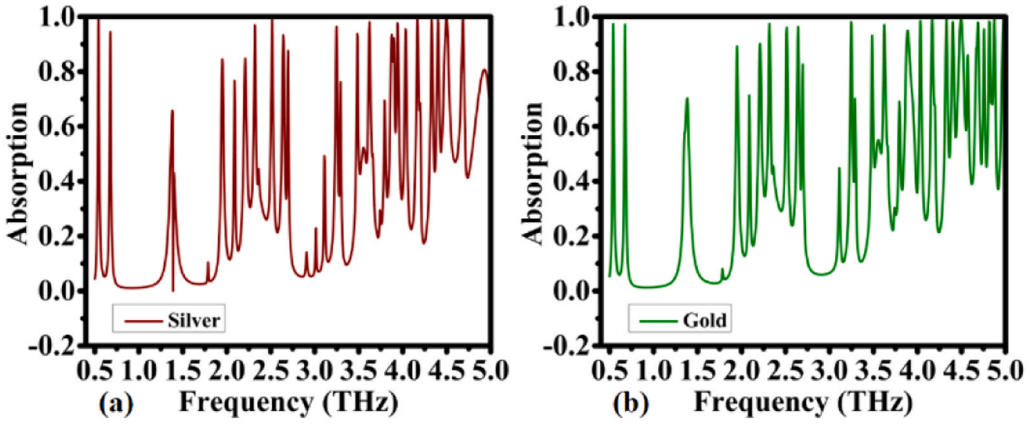

Fig. 8. Impact of resonator material selection on absorption: (a) Silver-based resonator; (b) Gold-based resonator.

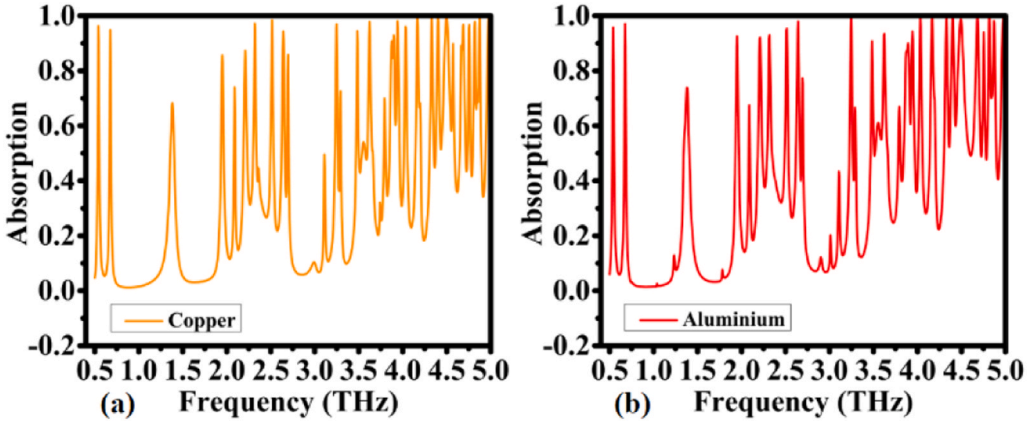

Fig. 9. Comparative absorption spectra for different resonator compositions: (a) Copper-based design; (b) Aluminum-based design.

4.5–5 THz range. In contrast, Fig. 11(b) shows that increasing the substrate thickness to 50 μm enhances absorption performance above 80%, particularly at 1.5 THz, between 2–3 THz, and within the 4–4.5 THz range. These results highlight a correlation between substrate thickness and absorption capability, with thicker substrates exhibiting strong absorption across the 0.5–5 THz frequency spectrum.

4. Structural optimization and enhancement of absorption properties

This section is concerned with evaluating the absorption characteristics, material effects, and electromagnetic response of the proposed metamaterial-based biosensor. By studying the real and imaginary components of the proposed absorber, we aim to understand various factors influencing the absorption efficiency and sensitivity. We also examine different electromagnetic properties, such as impedance, reflection coefficients, absorption efficiency, impedance, and S-

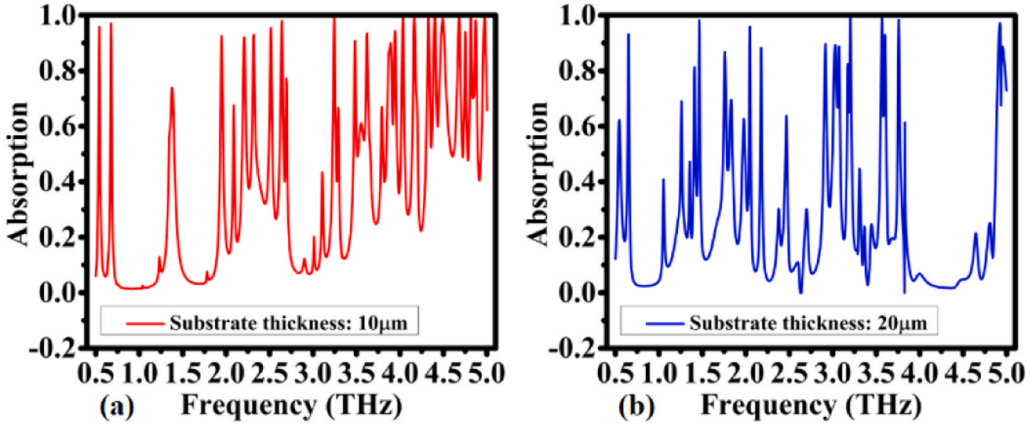

Fig. 10. Variation in absorption efficiency with substrate thickness: (a) 10 μm thick substrate; (b) 20 μm thick substrate.

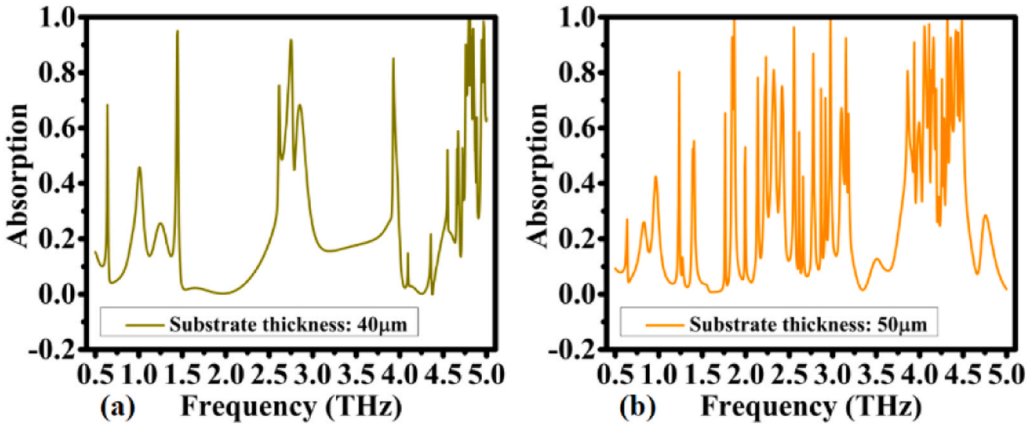

Fig. 11. Absorption characteristics under varying substrate thicknesses: (a) 40 μm thickness; (b) 50 μm thickness.

parameter to characterize the biosensor's potential for detection of PC-12 adrenal carcinoma cells.

4.1. Electromagnetic properties of the absorber

Permeability (μ) and permittivity (ε) play crucial roles in controlling the absorption properties of materials, particularly in their interaction with electromagnetic waves. To understand their significance, we studied the variation in the real and imaginary components of permeability and permittivity with respect to frequency. As illustrated in Fig. 12(a), the real components of permeability and permittivity exhibit significant fluctuations within the 0–5 THz frequency range. The real component of permeability, shown along the primary vertical axis, varies between −5 and 235 H/m, whereas the real component of permittivity, shown along the secondary vertical axis, ranges from −75–262 F/m. These broad variations highlight the metamaterial's strong electromagnetic response and its ability to efficiently control both electric and magnetic fields over a broad frequency range.

Several resonance peaks are observed within the considered frequency range for both permeability and permittivity, indicating strong interactions between the metamaterial and the incident electromagnetic waves. These interactions signify the multiband absorption

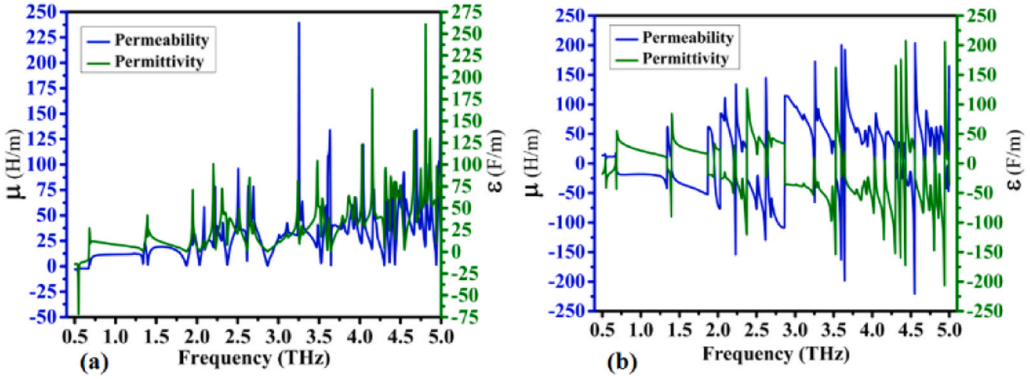

Fig. 12. Electromagnetic characteristics of the proposed absorber structure: (a) Real components of permeability (μ) and permittivity (ε); (b) Imaginary components of permeability (μ) and permittivity (ε).

characteristics of the metamaterial absorber. The maximum peak for the real part of μ, 235 H/m, is obtained at 3.29 THz, whereas the maximum peak for the real part of ε, 262 F/m, occurs at 4.81 THz. Moreover, the presence of negative values for μ and ε at a frequency of 0.5 THz is attributed to the negative refractive index property of the metamaterial. The occurrence of multiple peaks in the permeability and permittivity graph is essential for achieving optimal absorption within narrow frequency bands, thereby enhancing the sensor's sensitivity and selectivity across the 0–5 THz range.

Fig. 12(b) depicts the imaginary components of permeability (μ') and permittivity (ε'), which reflect the energy dissipation within the material due to magnetic and electric effects. These components are crucial for analyzing the metamaterial's absorption efficiency. Compared to the real part, a higher number of peaks are observed in the imaginary components of permeability and permittivity. It should be noted that the occurrence of negative values for μ' and ε' within the 0–0.5 THz range is due to the negative refractive index property of the metamaterial. The resonance peak positions in the imaginary component indicate efficient conversion of electromagnetic energy into heat, thereby reducing both reflection and transmission. The broad range of imaginary permittivity and permeability demonstrates the metamaterial's capability to absorb electromagnetic energy over a wide frequency spectrum, reinforcing its function as a perfect absorber. This property is particularly vital for biosensing applications, where precise absorption control is essential for detecting subtle biomolecular interactions at specific frequencies.

Subsequently, we investigated the impact of the real and imaginary components of the refractive index (RI) on the performance of the proposed structure, as depicted in Fig. 13(a). It is observed that the real part of the refractive index increases up to 63 as the frequency rises from 0.5 to 2.75 THz. The RI remains almost constant within the frequency range of 2.75–4.5 THz, after which it increases until 5 THz. On the other hand, the imaginary component of the refractive index exhibits multiple sharp peaks within the 0.5–5 THz range.

Fig. 13(b) displays the reflection coefficient (R) and absorption efficiency (A). The lower peak levels in the reflection spectra coincide exactly with the higher peaks of the absorption spectra. These multiple peaks in reflection and absorption highlight the ability of the proposed metamaterial absorber to achieve near-perfect absorption at resonance points. This high absorption efficiency, coupled with minimal reflection, is essential for sensitive biosensing applications, enabling the detection of molecular interactions across a wide range of frequencies.

4.2. Electromagnetic response and S-parameter investigation

Scattering parameter analysis is highly instrumental in metamaterial evaluation, as it provides focused insight into their overall electromagnetic behavior and sensing capabilities. S-parameters can describe how an electromagnetic wave propagates through and interacts with a biosensor, revealing essential details such as reflection, transmission, and absorption. By analyzing these parameters, it is possible to determine the resonance frequencies, absorption peaks, and observe shifts caused by biological interactions, enabling precise detection of biomolecules.

In this subsection, the final optimized metamaterial impedance and scattering parameters will be evaluated, with Fig. 14(a) starting with the real and imaginary parts of the normalized device impedance in relation to frequency, ranging from 500 GHz to 5 THz.

The real impedance exhibits a mild response, approaching the unitary value near the frequencies targeted for optimal matching at the desired absorbance peaks.

The second graph in Fig. 14(a) also shows the imaginary component, which clearly indicates most of the resonance frequencies through its sharp zero approaches or crossings, as expected.

The reflection coefficient was then evaluated, with Fig. 14(b) presenting the absolute value of the scattering parameter S_{11} (in dB) along with the achieved absorption rate realized by the metamaterial.

The design exhibited more than ten sharp resonances with reflection levels below −10 dB, an outstanding achievement for a sensor of this kind, with detection peaks spanning the entire spectrum, from as low as 0.6 THz to as high as 4.5 THz, allowing for a wide range of sensing applications, including the detection of PC-12 Adrenal Gland Carcinoma.

The absorption rate reflects both the low reflection rates and other internal phenomena, including the transmission coefficient. By considering all these contributions, the metamaterial-based sensor's absorption spectrum, shown in Fig. 14(b), demonstrates several peaks with very high absorption, including eight peaks with an absorption rate exceeding 0.99. It is also noteworthy that while absorption peaks are present throughout the spectrum, the most prominent ones are located at higher frequencies.

The sensor performance exhibits low sensitivity to moderate variations in the orientation and incidence angle of the terahertz waves due to the symmetric three-resonator metamaterial geometry and the impedance-matched absorber design. For oblique incidence within practical angular ranges, the primary effect is a small resonance frequency shift and minor reduction in absorption amplitude, while the multiband absorption behavior and sensing contrast are preserved. At extreme incidence angles, some polarization-dependent variations may occur; however, the fundamental sensing mechanism based on dielectric-induced resonance shifts remains stable. With excellent absorption and performance, the sensor was selected for further evaluation.

To better understand the internal workings of the proposed biosensor, the next section will provide a detailed analysis of the

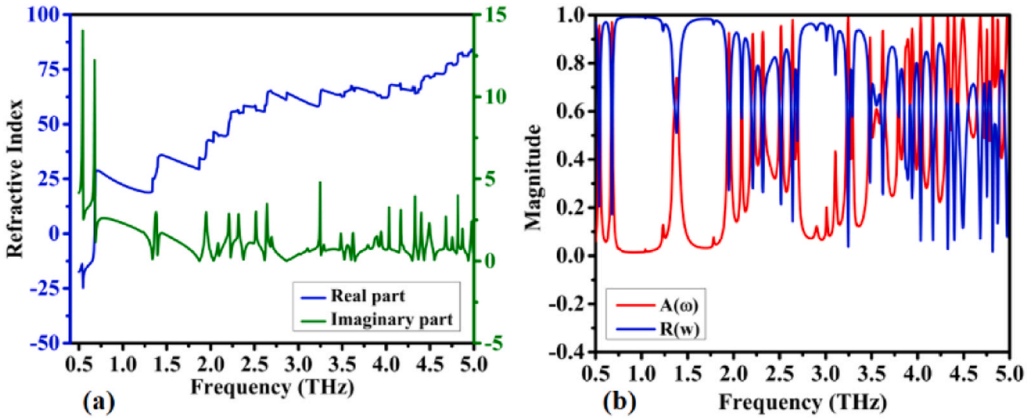

Fig. 13. Simulation-based evaluation of critical performance metrics: (a) Computed real and imaginary components of the refractive index; (b) Reflection coefficient and absorption efficiency analysis.

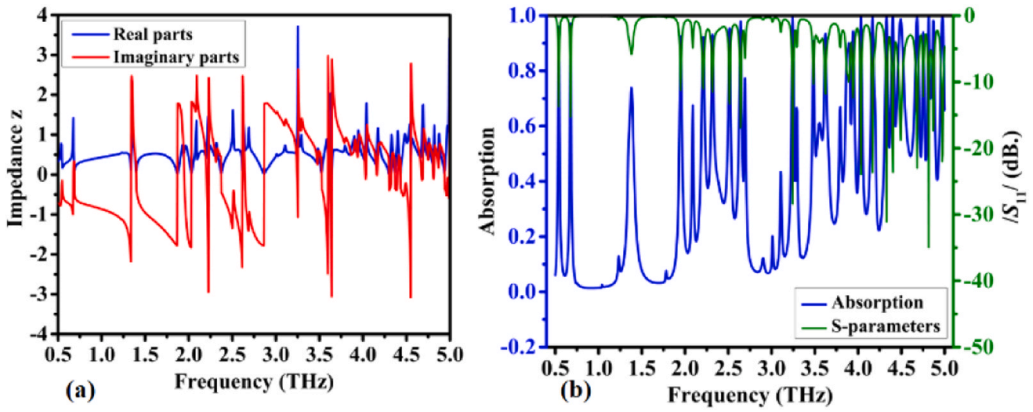

Fig. 14. Simulated response depicting absorber behavior: (a) Impedance characteristics; (b) S-parameter performance analysis (|S11| in dB).

electromagnetic fields and interactions occurring within the structure of the metamaterial, which generate the observed response.

5. Electromagnetic field and surface current distributions

The analysis of the electromagnetic (EM) field distribution in the designed metamaterial (MTM)-based biosensor provides a detailed understanding of the interaction between the biosensor structure and incident terahertz (THz) waves. The spatial distribution of the electric field (|E|), magnetic field (|H|), and surface current across the structure plays a critical role in determining the absorption efficiency and resonance characteristics of the biosensor. These distributions influence how the sensor interacts with different biological tissues, making it possible to achieve highly sensitive detection capabilities. The ability to manipulate and confine electromagnetic waves within the MTM structure is an essential factor for improving the sensor's overall performance.

5.1. Electric field distribution

The electric field distribution across the biosensor structure is crucial for understanding how energy is confined and absorbed. Figs. 15(a) and 15(b) illustrate the real and imaginary components of the |E|-field distribution, respectively. The real component of the |E|-field demonstrates the field intensity and interaction at different resonant frequencies, highlighting strong localization around the metallic resonators. This localization is *a* direct result of the coupling between the incident THz waves and the MTM structure, which enhances the sensor's ability to detect subtle biomolecular changes. The ability to confine electric fields in localized regions ensures efficient signal processing and improved accuracy in detecting biomolecular interactions.

The imaginary component of the |E|-field represents energy dissipation, which is associated with absorption losses in the resonator materials. High dissipation areas correspond to peak absorption frequencies, validating the sensor's high efficiency in THz wave absorption and conversion. This is particularly beneficial in biomedical applications where high sensitivity to minute changes in biological tissues is required. The electric field's confinement also plays a role in enhancing the quality factor (Q-factor) of the resonances, ensuring a sharper and more distinct absorption spectrum.

5.2. Magnetic field distribution

The magnetic field (|H|) distribution within the biosensor structure provides insights into the interaction between the resonator and the external THz field. Figs. 16(a) and 16(b) illustrate the real and imaginary components of the |H|-field, respectively. The real part of the |H|-field reveals strong confinement within the metallic regions, particularly in the areas surrounding the split-ring resonators, indicating enhanced energy storage and resonance behaviour. The localization of the magnetic field in these areas suggests that the sensor is highly responsive to variations in the surrounding dielectric properties, making it *a* suitable candidate for distinguishing between healthy and diseased tissues.

Conversely, the imaginary part of the |H|-field highlights the energy loss within the MTM structure, signifying the sensor's capability to

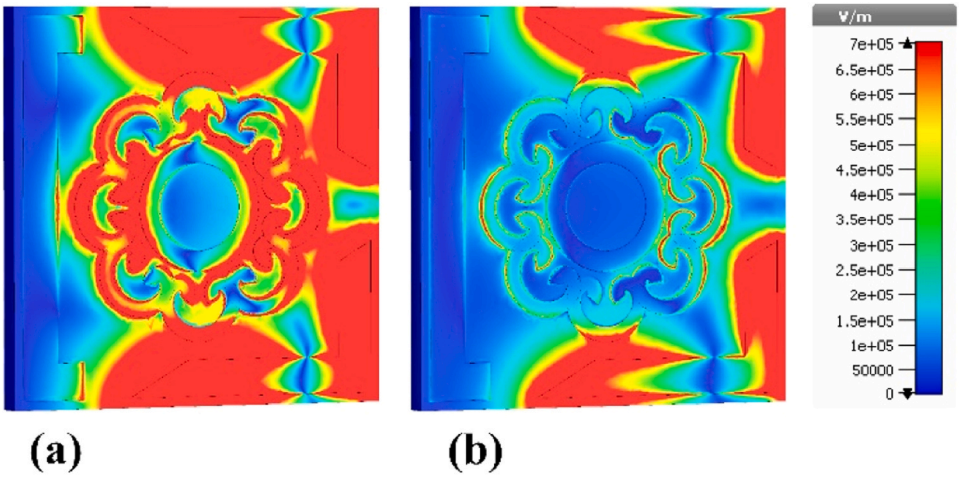

Fig. 15. Spatial representation of the electric field (|E|) distribution across the metamaterial structure: (a) Real component of the |E|-field; (b) Imaginary component of the |E|-field.

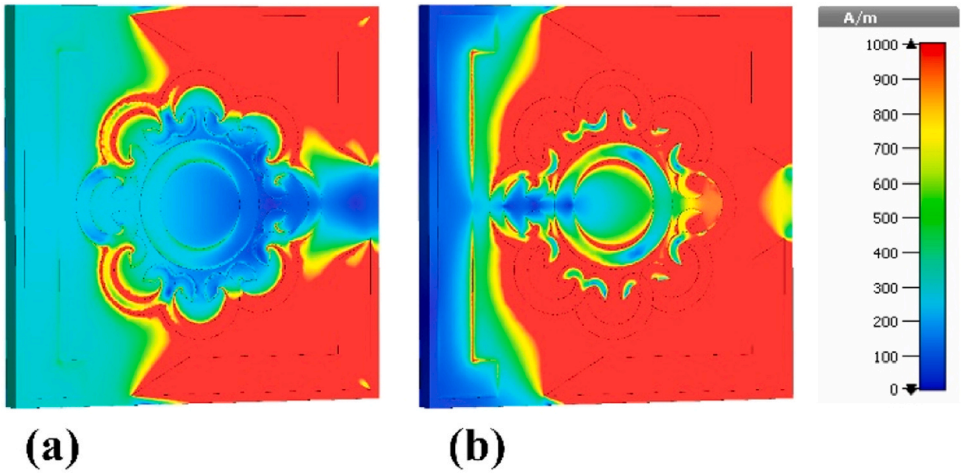

Fig. 16. Magnetic field (|H|) distribution mapping within the metamaterial structure: (a) Real component of the |H|-field; (b) Imaginary component of the |H|-field.

efficiently absorb and trap incident THz waves. The enhanced |H|-field intensities at specific resonant frequencies correlate directly with the observed absorption peaks, affirming the sensor's strong performance in THz biosensing applications. This behaviour is particularly advantageous in biosensors, where the ability to detect minute dielectric property changes is critical for accurate medical diagnoses. Additionally, the high-intensity magnetic fields indicate the presence of strong resonance modes, which contribute to the sensor's ability to selectively absorb targeted frequencies.

5.3. Surface current distribution

The surface current distribution is a key factor in characterizing the electromagnetic response of the biosensor. Figs. 17(a) and 17(b) present the real and imaginary components of the surface current distribution. The real component indicates a strong, localized current density in the metallic regions of the resonators, reinforcing the presence of dipole and quadrupole resonance modes. These resonance modes are crucial for generating multiple absorption peaks, ensuring that the biosensor can operate effectively across different THz frequency bands.

The imaginary part of the surface current distribution reflects energy dissipation due to resistive losses in the metallic structures, which contributes to the overall absorption efficiency of the biosensor. The alternating parallel and antiparallel surface current patterns observed in the structure support the generation of multiple absorption peaks in the THz spectrum. This multiband behaviour significantly enhances the biosensor's ability to detect various biomolecular interactions, making it a highly versatile diagnostic tool. The presence of strong surface currents at resonant frequencies also ensures efficient energy trapping, reducing unwanted radiation losses and improving the sensitivity of the sensor.

5.4. Significance of electromagnetic field analysis in biosensing

The detailed analysis of the electric and magnetic field distributions, along with surface current characteristics, confirms the robustness of the proposed biosensor in achieving high sensitivity and selectivity for biomolecular detection. The strong field confinement and optimized resonator design ensure minimal transmission losses and maximal absorption efficiency. This behaviour is critical for precise biomolecular interaction detection, allowing the biosensor to differentiate between normal and cancerous biological tissues. Additionally, the electromagnetic field analysis provides insights into how structural modifications can be used to further enhance biosensor performance by tailoring the resonance frequencies to target specific biomolecular interactions.

By leveraging these detailed field analyses, researchers can fine-tune the sensor's design to achieve optimal absorption and higher detection accuracy. The biosensor's ability to confine and manipulate electromagnetic waves efficiently ensures its applicability in a broad range of biomedical applications, including cancer detection, biomolecular diagnostics, and environmental monitoring.

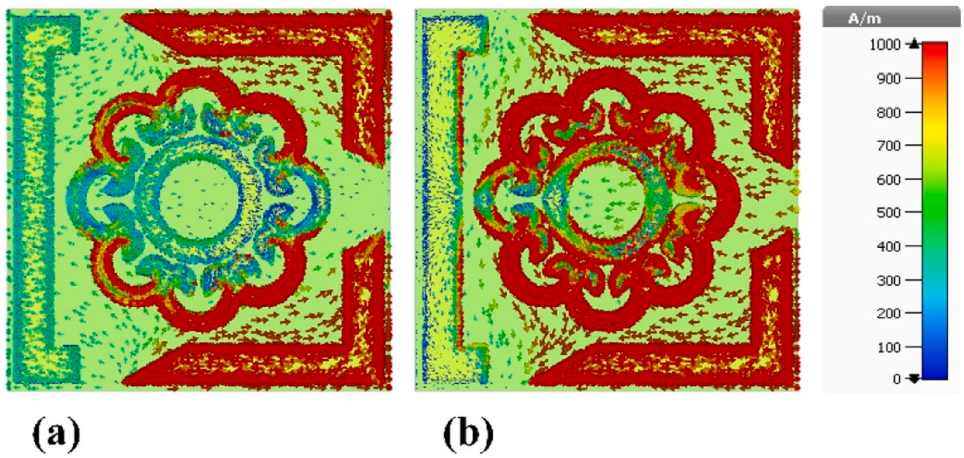

Fig. 17. Surface current distribution characteristics of the designed metamaterial: (a) Real component of the surface current; (b) Imaginary component of the surface current.

The electromagnetic field and surface current analysis validate the performance of the proposed MTM-based biosensor, making it a promising tool for highly sensitive, non-invasive biomedical diagnostics. Future improvements could involve exploring novel resonator geometries and material compositions to further enhance sensitivity and expand the range of detectable biomarkers.

6. Diagnosis of PC-12 adrenal gland cells carcinoma

The proposed terahertz multiband metamaterial biosensor demonstrates remarkable capability in distinguishing between healthy adrenal gland tissue and PC-12 adrenal carcinoma cells by exploiting its high sensitivity and broad operating range. Early-stage detection of adrenal gland carcinoma is critical for improving patient outcomes, and the biosensor's ability to detect minute dielectric differences between normal and cancerous tissues enhances its diagnostic utility.

In the present work, the sensor performance is evaluated through comprehensive full-wave electromagnetic simulations in CST, where healthy adrenal tissue and PC-12 carcinoma cells are represented using experimentally reported dielectric properties. The PC-12 cell layer was modeled with an 8 μm thickness, consistent with typical cellular monolayer dimensions used in terahertz biosensing studies. Complex permittivity values (including real and imaginary components) were implemented to account for realistic terahertz loss tangent and water-content-induced absorption effects.

The dielectric parameters were selected from published terahertz time-domain spectroscopy (THz-TDS) studies of hydrated biological tissues operating in the 0.5–5 THz range. In this regime, the real refractive index of biological tissues typically lies between 1.4 and 2.2, depending on hydration level and structural composition. Malignant tissues generally exhibit slightly elevated refractive indices and absorption coefficients due to increased water content and cellular density. The values used in this work fall within these experimentally reported ranges and were implemented using $n = \sqrt{\varepsilon_r}$.

This simulation-based approach enables systematic assessment of the sensing mechanism and performance trends under realistic biological conditions. Experimental validation using fabricated sensors and real biological samples is a natural next step and is part of ongoing and future work.

Fig. 18 illustrates the structure of the metamaterial (MTM) sensor, which consists of four layers designed for efficient interaction with terahertz (THz) waves. This layered design is essential for optimizing resonance characteristics and ensuring effective detection capabilities for distinguishing between healthy adrenal gland tissue and PC-12 adrenal carcinoma cells.

Fig. 19 presents the measured absorption spectra within the 0.5–5 THz range. Fig. 19(a) shows the response for healthy adrenal gland tissue, while Fig. 19(b) depicts the absorption profile of PC-12 adrenal carcinoma cells. A notable shift in absorption intensity and peak positioning is observed between these two cases, affirming the sensor's efficacy in biomolecular differentiation. The shift in absorption peaks suggests that terahertz waves interact differently with malignant cells due to changes in their molecular structure, water content, and cell membrane properties.

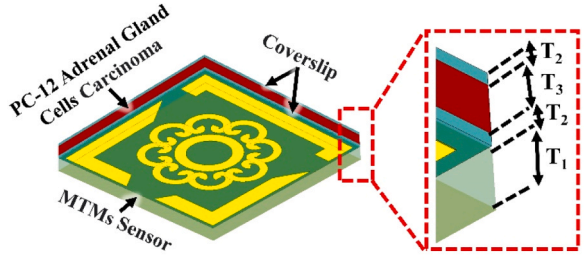

Fig. 18. Absorption coefficient analysis of the proposed biosensor for both healthy adrenal gland tissue and PC-12 adrenal carcinoma cells.

At present, there is no universally standardized calibration protocol for quantifying terahertz resonance shifts in biological samples, as measured responses depend on sample type, hydration level, and measurement configuration. In this work, calibration is implicitly achieved by using reference measurements (e.g., empty sensor or healthy tissue models) and quantifying relative resonance shifts induced by biological loading. In practical implementations, standardized calibration can be established through baseline referencing, controlled sample thickness, and calibration using known dielectric standards or reference biofluids.

The sensor distinguishes PC-12 carcinoma cells from other neuroendocrine or benign adrenal cells by detecting differences in their effective dielectric properties, which arise from variations in intracellular composition, membrane structure, and water content. PC-12 carcinoma cells exhibit distinct refractive-index and loss characteristics compared to benign cells, leading to measurable shifts in resonance frequency and absorption intensity across multiple terahertz bands. The multiband response of the metamaterial enables differential spectral analysis rather than reliance on a single resonance, improving discrimination reliability. When combined with reference measurements or pattern-based analysis, this spectral signature allows differentiation between malignant and non-malignant neuroendocrine cell types.

Fig. 20 highlights the application of microwave imaging (MWI) techniques for diagnosing PC-12 adrenal carcinoma. MWI is a powerful, non-invasive imaging method that provides real-time visualization of biological tissues based on their dielectric properties. The contrast in microwave response between healthy and cancerous samples reinforces the effectiveness of the biosensor in early-stage cancer detection. The ability to visualize changes in tissue composition at the cellular level offers a promising approach for identifying carcinoma at its earliest stages.

Figs. 21 and 22 present MWI-based visualizations of the electric field (E-field) and magnetic field (H-field) distributions, respectively. Figs. 21 (a) and 22(a) illustrate the field mapping for healthy adrenal gland tissue, while Figs. 21(b) and 22(b) depict the field interactions with PC-12 adrenal carcinoma cells. The variations in E-field and H-field intensities between these cases demonstrate the biosensor's ability to provide a distinct electromagnetic signature for different tissue types, further confirming its diagnostic potential. The E-field visualization highlights areas of strong interaction where terahertz radiation is absorbed by the biological tissue, whereas the H-field distribution provides insight into the overall magnetic response and wave propagation behavior within the sample.

In addition to its diagnostic accuracy, the biosensor's ability to operate over a wide frequency range allows for a comprehensive analysis of tissue composition and cellular abnormalities. The strong correlation between absorption characteristics and cellular composition opens new possibilities for integrating this technology into clinical oncology. Future work will involve refining the sensor's detection limits and enhancing its ability to differentiate between various cancer stages. Furthermore, the non-invasive nature of this approach makes it particularly suitable for frequent monitoring and early screening of adrenal gland carcinoma, potentially reducing the need for invasive biopsy procedures.

Overall, the application of this terahertz metamaterial biosensor in detecting PC-12 adrenal gland carcinoma cells demonstrates its potential as a transformative tool for cancer diagnostics. By leveraging absorption spectroscopy and microwave imaging, this approach provides a powerful means of identifying cancerous tissues with high precision, paving the way for further advancements in terahertz-based biomedical sensing.

Although terahertz sensing and MWI operate in different frequency regimes, both rely on contrast in the complex permittivity of biological tissues. In this work, MWI is not intended to directly validate the THz resonance mechanism, but rather to provide complementary

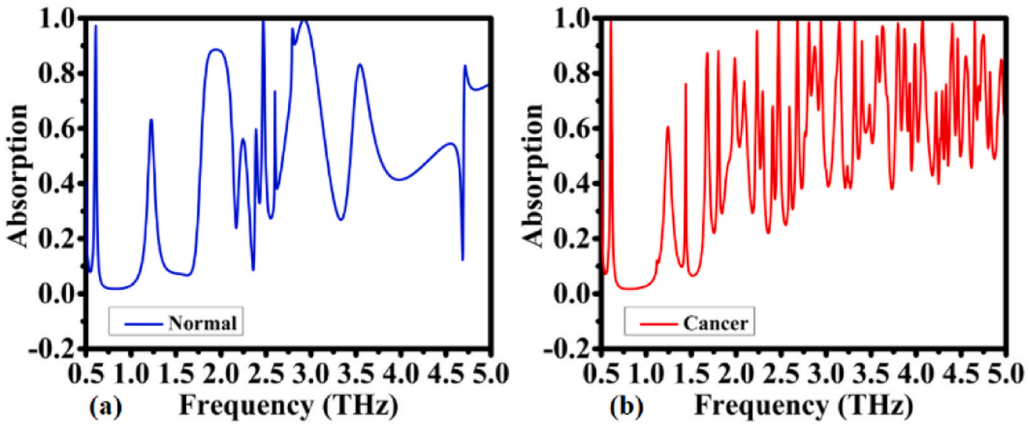

Fig. 19. Measured absorption spectra across the 0.5–5 THz range: (a) Healthy adrenal gland tissue; (b) PC-12 adrenal carcinoma cells.

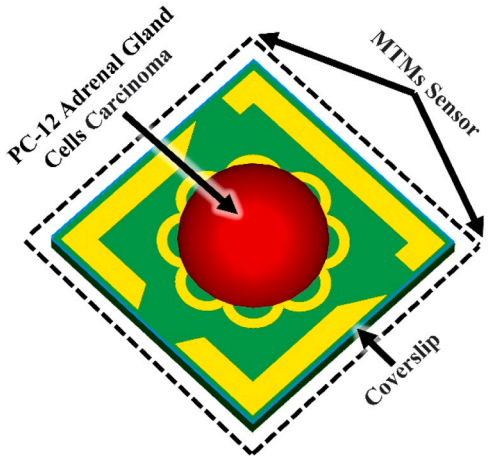

Fig. 20. Diagnosis of PC-12 adrenal carcinoma using microwave imaging (MWI) techniques.

confirmation that the assumed dielectric differences between healthy and cancerous tissues produce consistent electromagnetic contrast. While THz sensing probes near-field dielectric loading at micrometer scales, MWI visualizes macroscopic dielectric variations. Thus, the MWI results support the physical plausibility of the dielectric modeling used in the THz simulations.

7. Future perspective

The field of terahertz biosensing is rapidly evolving, and the proposed metamaterial-based micro-biosensor offers promising applications in early-stage cancer detection. Future research directions include:

1) Further optimization of metamaterial configurations and substrate materials can improve detection limits and biomolecular specificity. Future studies should explore alternative resonator designs and hybrid material compositions to enhance the sensor's resolution and absorption characteristics.
2) Beyond PC-12 adrenal carcinoma cells, the biosensor can be extended to detect other cancers and disease states that exhibit distinct terahertz dielectric signatures, such as breast, lung, cervical, or skin cancers. To adapt the sensor, modest modifications such as resonator geometry tuning, surface functionalization for target specificity, and optimization of the sample interface would be required.
3) The incorporation of AI-driven data analysis can enhance diagnostic accuracy by identifying subtle spectral variations. Deep learning algorithms can be trained on large datasets to detect cancerous signatures with high precision, reducing false positives and improving clinical decision-making.
4) Developing compact and wearable biosensor devices can enable real-time and point-of-care diagnostics. Advances in microfabrication and flexible electronics could facilitate the creation of biosensors that are lightweight, disposable, and easily deployable in remote or resource-limited settings. The biosensor can be implemented in point-of-care

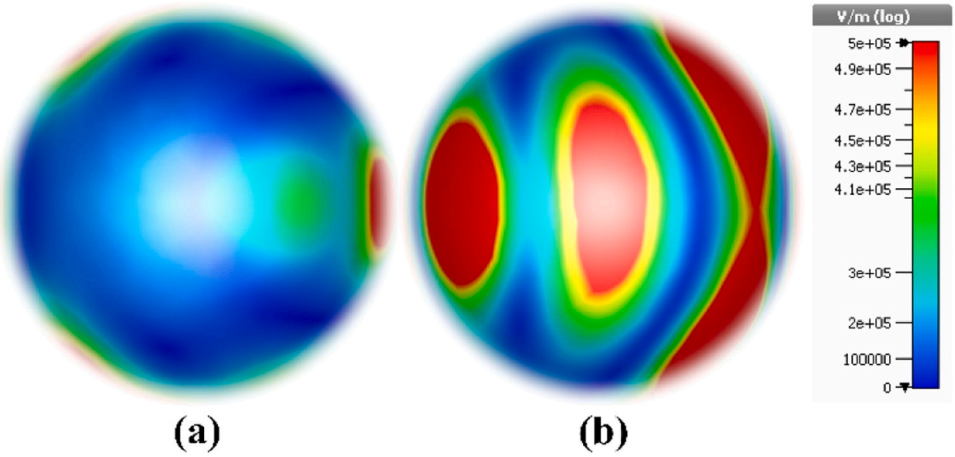

Fig. 21. Microwave imaging-based visualization of the electric field (|E|-field): (a) Healthy adrenal gland tissue; (b) PC-12 adrenal carcinoma cells.

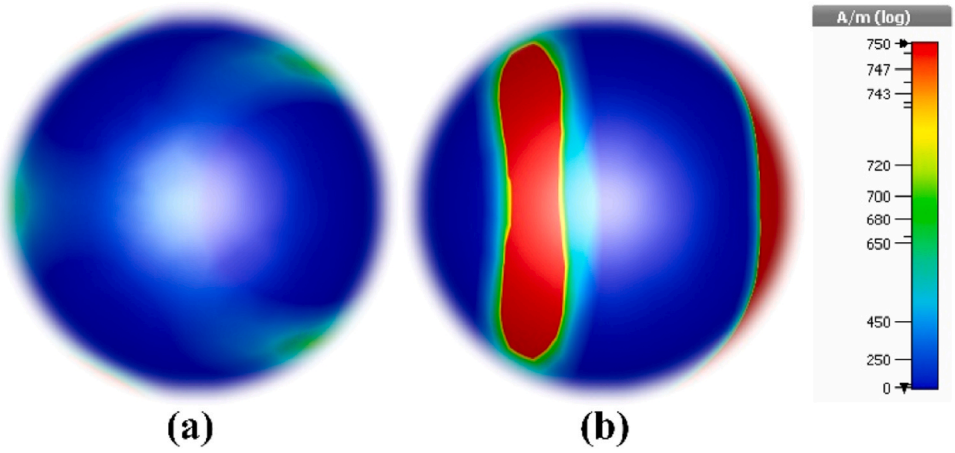

Fig. 22. Microwave imaging representation of the magnetic field (|H|-field): (a) Healthy adrenal gland tissue; (b) PC-12 adrenal carcinoma cells.

or handheld devices by integrating the miniaturized metamaterial chip into a disposable cartridge with simple sample handling, coupled to a compact terahertz source and detector. By monitoring resonance shifts or absorption changes at selected frequency bands, the system can operate with simplified electronics and minimal alignment, enabling rapid, portable diagnostics.

5) Extending the biosensor's functionality to detect multiple biomarkers simultaneously for comprehensive cancer screening. The design of multiband metamaterials could allow for the simultaneous detection of different cancer types, improving early diagnosis and treatment monitoring.
6) Extensive testing on patient-derived samples will be necessary to validate the sensor's performance in real-world medical applications. Large-scale clinical trials should be conducted to assess the biosensor's reliability, reproducibility, and diagnostic accuracy across diverse patient populations. Aluminum and PET are generally considered biocompatible and are widely used in biomedical and microfluidic devices; however, certain challenges may arise when interfacing them with living tissue or biofluids. Bare aluminum surfaces can undergo oxidation or ion release under prolonged exposure to ionic biofluids, which may affect surface stability and long-term measurements. PET, while chemically inert, can exhibit limited biofouling and nonspecific protein adsorption, potentially influencing sensing repeatability. These issues can be mitigated through surface passivation, thin dielectric coatings, or biocompatible functional layers, which are commonly employed in practical biosensor implementations.
7) Combining terahertz biosensing with other diagnostic modalities, such as infrared spectroscopy or Raman scattering, could enhance the overall robustness of the biosensor. Hybrid approaches may provide complementary insights into tissue pathology, improving the specificity and accuracy of cancer detection.
8) The transition from laboratory research to commercial deployment requires addressing regulatory challenges and manufacturing scalability. Collaboration with industry partners and healthcare providers can accelerate the biosensor's adoption in clinical practice, paving the way for future biomedical applications.

By addressing these future directions, terahertz metamaterial biosensors have the potential to revolutionize cancer diagnostics, enabling earlier detection, improved patient outcomes, and personalized treatment strategies. Continued interdisciplinary collaboration between engineers, biophysicists, and medical professionals will be key to unlocking the full potential of this groundbreaking technology.

The simulation results presented in this study are expected to be largely reproducible under realistic fabrication and biological testing conditions. The proposed biosensor employs micrometer-scale geometries and a simple Al/PET/Al configuration that is compatible with standard microfabrication techniques and tolerant to typical dimensional variations, which primarily lead to minor resonance shifts rather than degradation of absorption or sensing functionality. Moreover, the sensing mechanism relies on relative resonance shifts induced by effective refractive-index changes, making it robust against biological variability such as cell density and hydration. While practical measurements may exhibit slightly broadened resonances due to fabrication imperfections and material losses, the key multiband absorption behavior and sensing trends are expected to remain consistent.

Fabricating the proposed three-resonator metamaterial at a $150 \times 150\ \mu m^2$ scale requires precise lithographic patterning and alignment to preserve resonance accuracy, as well as uniform control of the thin aluminum layers and PET substrate thickness. Minor fabrication imperfections may introduce slight resonance shifts or peak broadening but are not expected to affect the fundamental multiband absorption behavior or sensing functionality.

Although this study is simulation-based, the proposed Al/PET/Al structure is compatible with standard microfabrication techniques such as photolithography or electron-beam lithography followed by thin-film aluminum deposition and lift-off patterning. Biological samples can be introduced using a controlled microfluidic channel or PDMS well to maintain an approximately 8 μm hydrated cell layer. The fabricated device can be characterized using terahertz time-domain spectroscopy (THz-TDS) in reflection mode, which is well suited for metamaterial perfect absorbers. Resonance shifts before and after biological loading can then be directly measured to quantify sensing performance. These established fabrication and measurement approaches support practical translation of the proposed biosensor.

8. Benchmarking

Benchmarking the performance of the proposed biosensor against existing THz-based biosensors provides insight into its competitive advantages and potential applications in biomedical diagnostics.

While many THz metamaterial sensors report multiband resonances, most operate over relatively narrow frequency ranges or exhibit moderate absorption efficiency and limited Q-factors. The specific gap addressed in this work is the simultaneous realization of broadband operation (0.5–5 THz), near-unity absorption at multiple discrete peaks, and strong near-field confinement within a compact Al/PET/Al perfect-absorber configuration tailored for PC-12 carcinoma detection. Unlike transmission-based or single-resonance designs, the impedance-matched architecture enables highly dispersive resonances that enhance refractive-index responsivity. A fair comparison with recent

Table 2
Breakthrough Advantages of the Proposed Biosensor.

Feature	Advantage
High Sensitivity	Exceptional sensitivity of 3906000 THz/RIU, enabling precise detection of minute biomolecular changes.
Broad Operating Range	Covers 0.5 – 5 THz, making it applicable for various biomolecular detections and material characterizations.
Multi-Peak Absorption	Offers absorption of > 99% (8 peaks), > 99.5% (6 peaks), > 99.8% (3 peaks), and > 99.9% (2 peaks), ensuring reliable detection.
Compact Design	Ultra-miniaturized structure (150 × 150 μm^2), suitable for integration into portable diagnostic devices.
High Figure of Merit (FOM)	Exceptional FOM of 181168831 RIU^{-1} , outperforming conventional biosensors.
Good Quality Factor (QF)	A QF of 28.279, enhancing spectral resolution and signal accuracy.
Simple Fabrication	Designed with three-layer aluminum-PET-aluminum structure, allowing cost-effective manufacturing.
Real-Time Detection	Capable of dynamic monitoring of biomolecular interactions in real-time.
Non-Invasive Approach	Uses terahertz radiation, which is non-ionizing, ensuring safer diagnostic applications.
Versatile Applications	Suitable for detecting cancer biomarkers, blood disorders, and other diseases.

Table 3
Advancing terahertz sensing for superior biomedical applications.

Novel Feature	Description
Metamaterial Perfect Absorber Design	Utilizes an optimized metamaterial structure to achieve near-perfect absorption across multiple resonance peaks.
Extremely High Sensitivity	Exhibits sensitivity orders of magnitude higher than most existing THz biosensors.
Multi-Resonance Peaks with High Absorption	Offers up to eight distinct resonance peaks with absorption exceeding 99%, ensuring superior detection capability.
Broadband Terahertz Operation	Covers a wide 0.5 – 5 THz frequency range, unlike conventional biosensors limited to narrowband operation.
Ultra-Compact Form Factor	Micro-sized (150 × 150 μm^2), making it among the smallest metamaterial-based biosensors for THz applications.
Enhanced Figure of Merit (FOM)	Achieves an unprecedented FOM of 181168831 RIU^{-1} , significantly higher than existing sensors.
Simple and Cost-Effective Fabrication	Consists of only three layers (Al-PET-Al), reducing complexity and fabrication costs.
Potential for Multiplexed Sensing	The multi-band response allows for the detection of multiple biomarkers simultaneously.
Strong Suitability for Cancer Detection	Specifically designed to detect biomarkers associated with early-stage cancer, particularly PC-12 adrenal gland carcinoma.
Non-Destructive and Biocompatible	Uses non-ionizing THz radiation, making it safer for biomedical applications.

state-of-the-art THz biosensors (Tables 4 and 5), using consistent definitions of sensitivity and FOM, demonstrates improvements in bandwidth, absorption strength, and dielectric loading sensitivity arising from optimized field–analyte overlap rather than structural complexity alone.

The proposed biosensor exhibits high sensitivity (3906000 THz/RIU), a figure of merit of 181168831 RIU^{-1} , and a quality factor of 28.279. The large FOM results from the combination of high sensitivity and extremely narrow FWHM values at specific resonances. The extracted FWHM values are on the order of 10^{-2}–10^{-3} THz at selected resonances, which significantly increases the calculated FOM.

For clarity, the refractive-index sensitivity is defined as:

$$S = \frac{\Delta f_{res}}{\Delta n} \tag{1}$$

where:

Table 4
Comparisons Of Bio-Sensing Performance Of Various Sensor Applications Based On THz Metamaterial.

References	Year Published	FOM (RIU−1)	Q	S (THz/RIU)	Bio-application
[79]	2014	0.1216	5.58	0.02432	Detection of Penicillia
[80]	2017	-	-	0.0242, 0.02438	Detection Of Virus
[81]	2020	-	-	0. 960	Biosensor, Collagen
[82]	2020	1.88	6.6	0.285	Sensor
[83]	2021	-	-	0. 2833	Polystyrene Particle
[84]	2022	1.81, 1.57	8.21, 6.05	0. 203	Sensor
[85]	2022	0.166	-	1.06	Detection of Avian Influenza Virus
[86]	2022	2.75	2.43	1.21	Cancer Diagnosi, Biosensor
[87]	2023	-	82	0.495	Cancer Detection
[47]	2023	0.86, 1.15	12.8, 13.5	0.0515, 0.076	Non-Melanoma Skin Cancer Diagnostics
[88]	2023	-	11	0.278	Bovin Serum Albumin Protein
[58]	2024	1.186, 4.656	7.81, 12.84	138, 440.5	Non-Melanoma Skin Cancer Diagnostics
This work	-	181168831	28.279	3906000	PC-12 Adrenal Gland Cells Carcinoma

- Δf_{res} is the resonance frequency shift (in THz)
- Δn is the change in refractive index (RIU).

The figure of merit is defined as:

$$\text{FOM} = \frac{S}{\text{FWHM}} \tag{2}$$

where:

- S is sensitivity (THz/RIU)
- FWHM is the full width at half maximum of the resonance peak (THz).

The high sensitivity enables detection of minute dielectric perturbations associated with early-stage pathological changes.

The exceptionally high sensitivity and FOM originate from the impedance-matched metamaterial perfect absorber configuration combined with strong near-field confinement in the analyte region. The Al/PET/Al architecture supports hybrid localized surface plasmon and Fabry–Pérot–type resonances, resulting in sharp, highly dispersive absorption peaks with near-unity absorption. Because the PC-12 cell layer is positioned directly within the region of maximum electric-field localization, small refractive-index perturbations induce comparatively large resonance shifts. Sensitivity is therefore amplified by both the high field–analyte overlap and the narrow resonance linewidths, rather than by numerical artifacts.

- Tables 2–5 illustrate key performance metrics, demonstrating that the proposed biosensor surpasses prior designs in terms of absorption efficiency, operational bandwidth, and biomolecular detection

Table 5
A Comparison Between The Terahertz Band Study On Perfect Metamaterials And The Recommended Biosensor.

References	Material substrate	Frequency operating THz	Absorptivity	Techniques used	Application
[89]	SiO_2	7–9.5	0.98	Au/SiO_2/ Graphene	Multi-Frequency Broadband and Ultra-Broadband
[90]	Silicon dioxide	1.5–1.7	0.972, 0.991	Gold/silicon dioxide/ Gold	Biosensor for Detecting Coronaviruses
[86]	SiO_2	0.5–2.5	-	SiO_2/Graphene	Breast Cancer Detection
[91]	SiO_2	2 −6	0.99	graphene/Au/SiO_2/Au	Refractive Index Sensor
[92]	Glass	0–0.37	0.998	Glass/InSb/MgF2/InSb	Colon Cancer Detection
[93]	Photonic crystal plate	1 −3	0.97, 0.98, 0.99	bulk Dirac semimetal/photonic crystal/Au	Narrowband Perfect Absorber
[94]	Dielectric layer	1 −3	0.99, 0.99	Au/dielectric layer/Au	Sensor
[95]	PET	0–3	0.99, 0.80, 0.95	PET/FSS/UV glue/ Graphene	Multifunctional Tunable Terahertz
[96]	Teflon	0.7–5	> 0.96	Ion gel/Graphene/Teflon/Gold	Polarization-Sensitive
[97]	Topas spacer	0.5 −4.5	0.99, 0.98, 0.99	graphene/Topas/Au	Ultra-Broadband Absorber
[98]	Dielectric Teflon	1 −2.2	0.99	Au/dielectric Teflon/Au	Sensor
This work	PET	0.5 −5	Eight peaks: > 0.99 Six peaks: > 0.995 Three peaks: > 0.998 Two peaks: > 0.999	Al/ PET /Al	PC-12 Adrenal Gland Cells Carcinoma

sensitivity. Compared to previously developed THz biosensors, the proposed design offers a broader frequency range, improved selectivity, and higher absorption efficiency.

- The biosensor's ultra-compact PET-based structure and aluminum resonator layer provide enhanced absorption across multiple THz peaks, ensuring high diagnostic accuracy. The choice of materials contributes to reduced fabrication costs while maintaining excellent mechanical stability and electrical performance.
- The biosensor operates efficiently over a wide THz spectrum (0.5–5 THz), allowing for multi-frequency analysis of biomolecular interactions. This capability makes it suitable for diverse biosensing applications, including cancer detection, virus identification, and protein analysis.
- Due to its excellent biocompatibility, non-invasive nature, and adaptability to real-time monitoring, this biosensor is a strong candidate for integration into clinical oncology diagnostics. The ability to detect PC-12 adrenal gland carcinoma cells with high precision positions this sensor as a potential alternative to traditional biopsy-based diagnostic methods.
- The sensor's simple three-layer aluminum-PET-aluminum structure enables cost-effective mass production. The manufacturing process can be adapted for large-scale fabrication using existing microfabrication techniques, making it feasible for commercial biomedical applications.
- Unlike many traditional biosensors that target a single biomarker, the proposed THz biosensor's multiband absorption capabilities allow for multiplexed sensing. This feature enhances its usability in detecting multiple cancer types or differentiating between various disease stages, improving diagnostic efficiency.
- The biosensor's performance could be further enhanced through the incorporation of advanced nanomaterials, such as graphene or quantum dots, to improve its sensitivity and selectivity. Additionally, integration with AI-based spectral analysis could further refine its diagnostic accuracy, making it an indispensable tool in modern medical diagnostics.

By establishing a clear comparison with existing biosensors and highlighting its unique advantages, this benchmarking analysis reinforces the transformative potential of the proposed THz biosensor in biomedical applications. The ability to achieve real-time, non-invasive, and highly accurate cancer detection makes this sensor a strong candidate for future adoption in clinical practice.

9. Conclusions

This study presents an innovative terahertz multiband metamaterial biosensor for the ultrasensitive detection of PC-12 adrenal gland carcinoma cells. The biosensor's optimized metamaterial architecture exhibits multiple high-absorption peaks, allowing precise differentiation between healthy and cancerous tissues. The integration of microwave imaging (MWI) further enhances its diagnostic capability by providing detailed electromagnetic field visualizations, demonstrating the sensor's high sensitivity and reliability.

The reported sensitivity and FOM describe the sensor's electromagnetic response and are not intended to replace clinical tools such as biopsies or imaging. Instead, the biosensor is envisioned as a complementary, non-invasive screening approach for early indication and risk stratification, with definitive diagnosis remaining reliant on established clinical methods.

Benchmarking analyses confirm that the proposed biosensor surpasses existing THz-based biosensors in terms of sensitivity, figure of merit, and operational bandwidth. Its compact structure, non-invasive approach, and real-time detection capabilities make it a promising tool for early-stage cancer diagnostics. The biosensor's exceptional performance is attributed to its advanced metamaterial configuration, enabling enhanced electromagnetic wave interaction for precise biomolecular detection.

In addition to its application in cancer diagnostics, the biosensor has the potential for broader biomedical applications, including the detection of viral pathogens, protein interactions, and blood disorder analysis. The ability to operate over a wide frequency range makes it adaptable for various medical and environmental sensing applications. The non-ionizing nature of terahertz radiation ensures that the biosensor is safe for repeated use in clinical settings, reducing the risks associated with conventional imaging techniques.

Future work will focus on refining the sensor's design, improving detection accuracy through AI integration, and conducting extensive clinical trials to validate its practical applications. Enhancements in material selection, including the incorporation of graphene-based or hybrid nanostructures, could further boost the sensor's selectivity and response time. Moreover, efforts will be directed towards developing portable, user-friendly diagnostic systems that integrate THz biosensing with real-time data processing for efficient disease monitoring and treatment planning.

The development of this terahertz metamaterial biosensor represents a significant advancement in biosensing technology. By leveraging its high sensitivity, non-invasiveness, and broad detection capabilities, this sensor has the potential to revolutionize early-stage cancer diagnostics

and other biomedical applications. With continued research and technological advancements, the proposed biosensor could become an essential tool in personalized medicine, enabling timely and accurate disease detection for improved patient outcomes.

CRediT authorship contribution statement

Hassan Zakeri: Writing – review & editing, Validation, Software, Conceptualization. **hmad Abbasi Nisar A:** Writing – review & editing, Validation, Data curation, Conceptualization. **Musa N. Hamza:** Writing – review & editing, Writing – original draft, Visualization, Validation, Software, Resources, Methodology, Investigation, Formal analysis, Data curation, Conceptualization. **Mohammad Alibakhshikenari:** Writing – review & editing, Writing – original draft, Visualization, Validation, Supervision, Software, Resources, Project administration, Methodology, Investigation, Funding acquisition, Formal analysis, Data curation, Conceptualization. **Bal Virdee:** Writing – original draft, Validation, Resources, Methodology, Data curation, Conceptualization. **Slawomir Koziel:** Writing – review & editing, Validation, Resources, Funding acquisition. **Syeda Iffat Naqvi:** Writing – review & editing, Visualization, Validation, Data curation. **Ali Farmani:** Writing – review & editing, Validation, Methodology. **Abinash Panda:** Writing – review & editing, Validation, Resources, Formal analysis. **Sunil Lavadiya:** Writing – review & editing, Validation, Formal analysis, Data curation. **Iftikhar ud Din:** Writing – review & editing, Validation, Software, Resources. **Bruno Sanches:** Writing – review & editing, Visualization, Validation, Data curation.

Funding

Co-funded by the European Union. Views and opinions expressed are however those of the author(s) only and do not necessarily reflect those of the European Union or the European Research Executive Agency. Neither the European Union nor the granting authority can be held responsible for them. Besides that, this publication has emanated from research jointly funded by Taighde Éireann – Research Ireland under Grant number 13/RC/2094_2, the European Union's Marie Sklodowska-Curie Actions under grant number 101126578 and was supported in part by University of Galway. In addition, this research has been supported by the Icelandic Research Fund (Grant No. 2410297) and the National Science Centre of Poland (Grant No. 2022/47/B/ST7/00072).

Declaration of Competing Interest

The authors declare that they have no known competing financial interests or personal relationships that could have appeared to influence the work reported in this paper.

Data availability

Data will be made available on request.

References

[1] M. Fassnacht, et al., Adrenocortical carcinomas and malignant phaeochromocytomas: ESMO–EURACAN clinical practice guidelines for diagnosis, treatment and follow-up, Ann. Oncol. 31 (11) (2020) 1476–1490.
[2] A. Berruti, et al., Adrenal cancer: ESMO clinical practice guidelines for diagnosis, treatment and follow-up, Ann. Oncol. 23 (2012) vii131–vii138.
[3] A.J. Sedlack, et al., Preclinical models of adrenocortical cancer, Cancers 15 (11) (2023) 2873.
[4] C. Jimenez, S. Fazeli, A. Román-Gonzalez, Antiangiogenic therapies for pheochromocytoma and paraganglioma, Endocr. Relat. Cancer 27 (7) (2020) R239–R254.
[5] S. Nölting, et al., Personalized management of pheochromocytoma and paraganglioma, Endocr. Rev. 43 (2) (2022) 199–239.
[6] D. Press, et al., Predictors of recurrence in pheochromocytoma, Surgery 156 (6) (2014) 1523–1528.
[7] A.K.-y Lam, Update on adrenal tumours in 2017 World Health Organization (WHO) of endocrine tumours, Endocr. Pathol. 28 (2017) 213–227.
[8] S. Yu, D. Dolezal, H.R. Aslanian, G. Cai, Fine-needle aspiration biopsy of adrenal gland lesions: the roles of image guidance, rapid on-site evaluation and additional tissue sampling, Cytopathology (2025).
[9] A. Angelousi, et al., The role of immunohistochemical markers for the diagnosis and prognosis of adrenocortical neoplasms, J. Pers. Med. 11 (3) (2021) 208.
[10] W. Gan, X. Han, Y. Gong, Y. Yang, C. Wang, Z. Zhang, Diagnostic and prognostic assessments of adrenocortical carcinomas by pathological features, immunohistochemical markers and reticular histochemistry staining, Diagn. Pathol. 19 (1) (2024) 71.
[11] C. Mytareli, et al., Evaluation of microRNAs as liquid biopsy markers in adrenocortical tumors, Front. Endocrinol. 16 (2025) 1511520.
[12] J. Datta, R.E. Roses, Surgical management of adrenocortical carcinoma: an evidence-based approach, Surg. Oncol. Clin. 25 (1) (2016) 153–170.
[13] Y. Tang, Z. Liu, Z. Zou, J. Liang, Y. Lu, Y. Zhu, Benefits of adjuvant mitotane after resection of adrenocortical carcinoma: a systematic review and meta-analysis, BioMed. Res. Int. 2018 (1) (2018) 9362108.
[14] M. Fassnacht, et al., Combination chemotherapy in advanced adrenocortical carcinoma, N. Engl. J. Med. 366 (23) (2012) 2189–2197.
[15] V. Srougi, et al., Adjuvant radiotherapy for the primary treatment of adrenocortical carcinoma: are we offering the best? Int. Braz. J. Urol. 43 (05) (2017) 841–848.
[16] B. Bracci, et al., Adrenal lesions: a review of imaging, Diagnostics 12 (9) (2022) 2171.
[17] M. Barat, et al., Adrenal mass characterization in the era of quantitative imaging: state of the art, Cancers 14 (3) (2022) 569.
[18] N. Singh, K.K. Thakur, S. Moidu, N. Anand, Incidental detection of purely cystic pheochromocytoma in a young adult presenting with lower urinary tract infection, Radiol. Case Rep. 19 (12) (2024) 6152–6156.
[19] S.Y. Woo, S. Park, K.Y. Kwon, D.-M. Lim, K.-Y. Park, J.-D. Kim, Ruptured triple hormone-secreting adrenal cortical carcinoma with hyperaldosteronism, hypercortisolism, and elevated normetanephrine: a case report, J. Yeungnam Med. Sci. 41 (4) (2024) 306–311.
[20] F. Cioppi, et al., Targeted next generation sequencing molecular profiling and its clinical application in adrenocortical cancer, Eur. J. Endocrinol. 191 (1) (2024) 17–30.
[21] M. Scatolini, et al., Germline NGS targeted analysis in adult patients with sporadic adrenocortical carcinoma, Eur. J. Cancer 205 (2024) 114088.
[22] D. Oprea, C.G. Sanz, M.M. Barsan, T.A. Enache, PC-12 cell line as a neuronal cell model for biosensing applications, Biosensors 12 (7) (2022) 500.
[23] A. Sundin, E. Hindié, A.M. Avram, A. Tabarin, K. Pacak, D. Taïeb, A clinical challenge: endocrine and imaging investigations of adrenal masses, no. Supplement 2, J. Nucl. Med. 62 (2021) 26S–33S.
[24] M.J. Metman, et al., Outcomes after surgical treatment of metastatic disease in the adrenal gland; valuable for the patient? Cancers 14 (1) (2021) 156.
[25] O.A. Shariq, T.J. McKenzie, Adrenocortical carcinoma: current state of the art, ongoing controversies, and future directions in diagnosis and treatment, Ther. Adv. Chronic Dis. 12 (2021) 20406223211033103.
[26] A. Tiwari, R. Trivedi, S.-Y. Lin, Tumor microenvironment: barrier or opportunity towards effective cancer therapy, J. Biomed. Sci. 29 (1) (2022) 83.
[27] O. Elhanani, R. Ben-Uri, L. Keren, Spatial profiling technologies illuminate the tumor microenvironment, Cancer Cell 41 (3) (2023) 404–420.
[28] Q. Zhao, J. Zhou, F. Zhang, D. Lippens, Mie resonance-based dielectric metamaterials, Mater. Today 12 (12) (2009) 60–69.
[29] M.-R. Nickpay, M. Danaie, A. Shahzadi, Graphene-based tunable quad-band fan-shaped split-ring metamaterial absorber and refractive index sensor for THz spectrum, Micro Nanostruct. 173 (2023) 207473.
[30] W. Han, et al., Selectable Narrow-Band Anisotropic Perfect Absorbers Based on α-MoO 3 Metamaterials for Refractive Index Sensing, IEEE Sens. J. (2025).
[31] M.N. Hamza, et al., Development of a High-Sensitivity Triple-Band Nano-Biosensor Utilizing Petahertz Metamaterials for Optimal Absorption in Early-Stage Leukemia Detection, IEEE Sens. J. (2025).
[32] S. Ahmed, T. Alam, P. Kirawanich, M.J. Singh, M.T. Islam, Highly sensitive circle enclosed D-pad resonator-based narrowband Metamaterial Absorber for biosensing applications, IEEE Sens. J. (2025).
[33] S. Yin, H. Zhong, W. Huang, W. Zhang, Deep learning enabled design of terahertz high-Q metamaterials, Opt. Laser Technol. 181 (2025) 111684.
[34] M.N. Hamza, et al., Precision multi-band terahertz metamaterial biosensor with targeted spectral selectivity for early detection of MCF-7 breast cancer cells, IEEE Sens. J. (2025).
[35] W. Wang, Q. Wu, H. Li, M. Li, Numerical research on terahertz hyperbolic metamaterials composed of interlaced graphene-dielectric multilayers and a microcavity, Opt. Laser Technol. 181 (2025) 111793.
[36] M.K. Uddin, et al., Polarization insensitive U-coupled splits ring resonator-based hexa-band metamaterial absorber for concentration of solid material sensing applications, Opt. Laser Technol. 181 (2025) 111975.
[37] M.N. Hamza, et al., Design of a high-sensitivity MTM-based multi-band micro-biosensor for early-stage non-melanoma skin cancer diagnosis in the terahertz region, Opt. Laser Technol. 192 (2025) 114015.
[38] J. Li, H. Chen, S.L. Yap, B. Zhang, A temperature-insensitive graphene-water-based ultra-wideband terahertz metamaterials absorber designed using deep neural networks, Opt. Laser Technol. 185 (2025) 112591.
[39] M.A. Khalil, et al., A compact tri-octagonal negative indexmetamaterial sensor for liquid adulteration detection, Opt. Laser Technol. 184 (2025) 112499.

[40] M.N. Hamza, et al., Development of a Terahertz metamaterial micro-biosensor for ultrasensitive multispectral detection of early-stage cervical cancer, IEEE Sens. J. (2024).
[41] H. Jiang, B. Wang, Z. Liu, New dual-peak High-performance structure utilizing terahertz metamaterial metasurface for concentration detection of H2 and CH4 gases, Opt. Laser Technol. 186 (2025) 112728.
[42] H. Hu, H. Zhang, H. Jiang, Z. Cui, Y. Wang, D. Wu, Tunable multifunctional terahertz metamaterial device based on metal-dielectric-vanadium dioxide, Opt. Laser Technol. 181 (2025) 111629.
[43] M.N. Hamza, M.T. Islam, S. Koziel, Advanced sensor for non-invasive breast cancer and brain cancer diagnosis using antenna array with metamaterial-based AMC, Eng. Sci. Technol. Int. J. 56 (2024) 101779.
[44] H. Sun, et al., Terahertz perfect metasurface absorber based on groove-ring-shaped Ti 3C 2 T x MXene for refractive index sensing application, IEEE Sens. J. (2025).
[45] X. Zhang, Z. Wang, Y. Gong, Progress in multifunctional tunable Terahertz metasurface waveplates, J. Electron. Mater. (2025) 1–22.
[46] W. Wang, G. Li, G. Yang, D.W. Schubert, Enhanced multifunctionality of carbon black-modified melamine sponge: flame retardancy, electromagnetic wave absorption, and sensing capabilities, J. Electron. Mater. 54 (3) (2025) 2111–2121.
[47] M.N. Hamza, M.T. Islam, Designing an extremely tiny dual-band biosensor based on MTMs in the Terahertz region as a perfect absorber for non-melanoma skin cancer diagnostics, IEEE Access 11 (2023) 136770–136781.
[48] Y. Tong, et al., Design and analysis of Terahertz wave all-dielectric grating magnetic reflector, J. Electron. Mater. (2025) 1–11.
[49] S. Sharma, A. Kumar, T.S. Saini, Design and simulation of a Terahertz sensor for blood components detection using photonic crystal fiber: S. Sharma et al, J. Electron. Mater. (2025) 1–13.
[50] M.N. Hamza, et al., Designing a High-sensitivity Microscale Triple-band Biosensor based on Terahertz MTMs to provide a perfect absorber for Non-Melanoma Skin Cancer diagnostic, IEEE Photonics J. (2024).
[51] Y. Liu, et al., Temperature and Refractive Index THz Sensor Based on All-Dielectric InSb Metasurfaces: Y. Liu et al, J. Electron. Mater. (2025) 1–12.
[52] B. Li, et al., Ultra-broadband and wide-angle metamaterial absorber based on vertical three-square patches structure gallium nitride for terahertz wave, J. Electron. Mater. (2025) 1–11.
[53] M.N. Hamza, et al., Terahertz dual-band metamaterial biosensor for cervical-cancer diagnostics, IEEE Photonics J. (2024).
[54] O. Elalaouy, S. Das, M. El Ghzaoui, A.D. Algarni, B.T.P. Madhav, J. Foshi, An ultra-thin polarization-sensitive quad-band metamaterial absorber (QMMA) with ten absorption peaks for diversified advanced millimeter-wave wireless applications, J. Electron. Mater. (2025) 1–20.
[55] M.N. Hamza, S. Koziel, A. Pietrenko-Dabrowska, Design and experimental validation of a metamaterial-based sensor for microwave imaging in breast, lung, and brain cancer detection, Sci. Rep. 14 (1) (2024) 16177.
[56] Y. Zheng, Y. Chen, Y. Xu, Toroidal dipole all-dielectric metasurfaces with high sensitivity, high figure of merit, and robustness for refractive index sensing, J. Electron. Mater. 53 (2) (2024) 674–682.
[57] A. Teber, A dual-band terahertz metamaterial absorber using an all-metal aluminum hexagonal metasurface structure for sensing of cancerous cells, J. Electron. Mater. 53 (5) (2024) 2686–2701.
[58] M.N. Hamza, M.T. Islam, S. Lavadiya, S. Koziel, I. Ud Din, B. Sanches, Designing a High-sensitivity Dual-band Nano-Biosensor based on Petahertz MTMs to provide a perfect absorber for Early-Stage Non-Melanoma Skin Cancer diagnostic, IEEE Sens. J. (2024).
[59] G. Thenuwara, B. Javed, B. Singh, F. Tian, Biosensor-enhanced organ-on-a-chip models for investigating glioblastoma tumor microenvironment dynamics, Sensors 24 (9) (2024) 2865.
[60] M.N. Hamza, et al., Terahertz Nanophotonic Hybrid-Metal Biosensor for Ultrasensitive, Noninvasive Cancer Detection Via Exosome Biomarkers, J. Electron. Mater. (2025) 1–24.
[61] S. Ganesh, K. Venkatakrishnan, B. Tan, Early detection and prediction of cancer metastasis–Unravelling metastasis initiating cell as a dynamic marker using self-functionalized nanosensors, Sens. Actuators B Chem. 361 (2022) 131655.
[62] M.N. Hamza, M.T. Islam, Design of MTM-based Multi-band Micro-Biosensor in Terahertz region as perfect absorber for Early-Stage Leukemia Diagnosis with sensitivity 18626373 THz/RIU, IEEE Sens. J. (2024).
[63] M. Amiri, M. Abolhasan, N. Shariati, J. Lipman, Development of a polarization-neutral metamaterial absorber for efficient low-power EM energy harvesting, Sens. Actuators A Phys. 381 (2025) 116055.
[64] M.N. Hamza, et al., High-sensitivity nanometamaterial near-infrared biosensor for label-free early cancer detection via exosomal biomarkers, Appl. Opt. 65 (1) (2025) 39–54.
[65] M.Z.B. Chowdhury, M.T. Islam, M.A. Alawad, M. Ouda, A.M. Alenezi, Design and Practical Evaluation of a Dual-Band Dispersion-Engineered Metamaterial Sensor for Sensing Applications, Sens. Actuators A Phys. (2026) 117515.
[66] S. Douhi, Y. Houssaini, S. Das, V. Subramanian, B.T.P. Madhav, A. Eddiai, Metamaterial-integrated wearable UWB antenna with SAR reduction and gain enhancement for Wireless Body Area Sensor Networks (WBASNs): Design and experimental verification, Sens. Actuators A Phys. 388 (2025) 116499.
[67] Q. Tian, G. Huang, X. Li, J. Li, Design and measurement of a terahertz dual-absorption mode metamaterial and its temperature sensing performance, Sens. Actuators A Phys. (2025) 117226.
[68] M.N. Hamza, et al., Nanophotonic perfect absorber with ultra-broadband terahertz-to-infrared response via hybrid-material design for advanced optical sensing, PloS One 21 (2) (2026) e0342168.
[69] M. Zhong, Verification of a metamaterial sensor strategy to measure the effect of the acoustic wave on the transmission properties of the optical fiber, Sens. Actuators A Phys. (2025) 116861.
[70] K. Khandakar, M.O. Faruk, A.I. Ferdous, M.N.R. Naim, Terahertz Photonic Crystal Fiber Sensor for Cancer Cell Detection: Performance Analysis and Discrimination, Cancer Med. 14 (13) (2025) e71024.
[71] D. Kundu, et al., Early Brain Tumour Cell Detection With High-Sensitivity Terahertz Sensors Based on Photonic Crystal Fibre, IET Nanodielectrics 8 (1) (2025) e70008.
[72] M.M. Bani, K.S. Noor, A.I. Ferdous, M.S. Anower, High-performance photonic crystal fibre biosensor for identifying Jurkat cells by refractive index analysis, IET Nanodielectrics 7 (4) (2024) 282–295.
[73] M.N.R. Naim, J.T. Upoma, A.I. Ferdous, K. Khandakar, M.G. Sadeque, M.S. Rana, Terahertz spectrum-based refractive index sensor for brain lesion detection using photonic crystal fibers, Plos One 20 (3) (2025) e0320355.
[74] A. Iftekharul Ferdous, K. Khandakar, S. Hossain, K.S. Noor, M.M. Eid, A.N. Z. Rashed, Innovative high sensitivity, selectivity, and low birefringence limit based blood cell detection in terahertz spectrum with octagonal core refractive index sensing, Appl. Phys. A 131 (4) (2025) 324.
[75] A.I. Ferdous, et al., Photonic crystal fiber-based terahertz biosensor: Identifying Staphylococcus aureus bacteria and skin health implications, Array (2025) 100580.
[76] A.I. Ferdous, et al., Development and enhancement of PCF-based sensors for terahertz-frequency region breast cancer cell detection, Cell Biochem. Biophys. 82 (3) (2024) 2837–2852.
[77] A. Iftekharul Ferdous, M.S. Islam, K.S. Noor, M.M. Bani, N.U. Badhon, M. Enzamam-Ul-Haque, Harnessing THz technology: biosensor for highly accurate cervical cancer cell detection via refractive index, Cell Biochem. Biophys. 82 (3) (2024) 2095–2106.
[78] D. Kundu, et al., Optimized PCF architectures for THz detection of aquatic pathogens: Enhancing water quality monitoring, PloS One 20 (1) (2025) e0317533.
[79] S. Park, et al., Detection of microorganisms using terahertz metamaterials, Sci. Rep. 4 (1) (2014) 4988.
[80] S. Park, S. Cha, G. Shin, Y. Ahn, Sensing viruses using terahertz nano-gap metamaterials, Biomed. Opt. Express 8 (8) (2017) 3551–3558.
[81] S. Asgari, N. Granpayeh, T. Fabritius, Controllable terahertz cross-shaped three-dimensional graphene intrinsically chiral metastructure and its biosensing application, Opt. Commun. 474 (2020) 126080.
[82] T. Chen, D. Zhang, F. Huang, Z. Li, F. Hu, Design of a terahertz metamaterial sensor based on split ring resonator nested square ring resonator, Mater. Res. Express 7 (9) (2020) 095802.
[83] J. Yang, Y.-S. Lin, Design of tunable terahertz metamaterial sensor with single-and dual-resonance characteristic, Nanomaterials 11 (9) (2021) 2212.
[84] H. Hu, B. Qi, Y. Zhao, X. Zhang, Y. Wang, X. Huang, A graphene-based THz metasurface sensor with air-spaced structure, Front. Phys. 10 (2022) 990126.
[85] E. Hoseini, A. Mir, A. Farmani, Modeling and proposal of a black phosphorus-based nanostructure for detection of avian influenza virus in infrared region, Opt. Quantum Electron. 54 (10) (2022) 609.
[86] C. Tan, et al., Cancer diagnosis Using Terahertz-graphene-metasurface-based biosensor with dual-resonance response, Nanomaterials 12 (21) (2022) 3889.
[87] Z. Mezache, Z. Hafdi, J. Tao, Design of a novel graphene buzzle metamaterial refractometer for sensing of cancerous cells in the terahertz regime, Optik 287 (2023) 171170.
[88] Y. Shen, et al., Low-concentration biological sample detection using an asymmetric split resonator Terahertz metamaterial, Photonics 10 (2) (2023) 111.
[89] Z. Chen, et al., Graphene multi-frequency broadband and ultra-broadband Terahertz absorber based on surface plasmon resonance, Electronics 12 (12) (2023) 2655.
[90] Z. El-Wasif, T. Ismail, O. Hamdy, Design and optimization of highly sensitive multi-band terahertz metamaterial biosensor for coronaviruses detection, Opt. Quantum Electron. 55 (7) (2023) 604.
[91] M.-R. Nickpay, M. Danaie, A. Shahzadi, Highly sensitive THz refractive index sensor based on folded split-ring metamaterial graphene resonators, Plasmonics (2021) 1–12.
[92] Z. Vafapour, W. Troy, A. Rashidi, Colon cancer detection by designing and analytical evaluation of a water-based THz metamaterial perfect absorber, IEEE Sens. J. 21 (17) (2021) 19307–19313.
[93] Y. Wang, et al., Terahertz tunable three band narrowband perfect absorber based on Dirac semimetal, Phys. E Low-dimensional Sys. Nanostruct. 131 (2021) 114750.
[94] B.-X. Wang, Y. He, P. Lou, W. Xing, Design of a dual-band terahertz metamaterial absorber using two identical square patches for sensing application, Nanoscale Adv. 2 (2) (2020) 763–769.
[95] S. Zhuang, et al., Graphene-based absorption–transmission multi-functional tunable THz metamaterials, Micromachines 13 (8) (2022) 1239.
[96] S. Asgari, T. Fabritius, Numerical simulation and equivalent circuit model of multi-band Terahertz absorber composed of double-sided graphene comb resonator array, IEEE Access (2023).
[97] L. Liu, W. Liu, Z. Song, Ultra-broadband terahertz absorber based on a multilayer graphene metamaterial, J. Appl. Phys. 128 (9) (2020).
[98] A.S. Saadeldin, M.F.O. Hameed, E.M. Elkaramany, S.S. Obayya, Highly sensitive terahertz metamaterial sensor, IEEE Sens. J. 19 (18) (2019) 7993–7999.